NAVAL POSTGRADUATE SCHOOL

MONTEREY, CALIFORNIA

THESIS

INVESTIGATION OF ULTRA HIGH MOLECULAR WEIGHT POLYETHYLENE (UHMWPE) TEXTILE BACKING SYSTEMS INTEGRATED WITH CERAMIC SPHERE BODY ARMOR SYSTEMS

by

Brent W. Morrison

December 2021

Thesis Advisor: Raymond M. Gamache
Second Reader: Abram H. Clark IV

THIS PAGE INTENTIONALLY LEFT BLANK

REPORT DOCUMENTATION PAGE	*Form Approved OMB No. 0704-0188*

1. AGENCY USE ONLY *(Leave blank)*	**2. REPORT DATE** December 2021	**3. REPORT TYPE AND DATES COVERED** Master's thesis

4. TITLE AND SUBTITLE
INVESTIGATION OF ULTRA HIGH MOLECULAR WEIGHT POLYETHYLENE (UHMWPE) TEXTILE BACKING SYSTEMS INTEGRATED WITH CERAMIC SPHERE BODY ARMOR SYSTEMS

5. FUNDING NUMBERS

6. AUTHOR(S) Brent W. Morrison

7. PERFORMING ORGANIZATION NAME(S) AND ADDRESS(ES)
Naval Postgraduate School
Monterey, CA 93943-5000

8. PERFORMING ORGANIZATION REPORT NUMBER

9. SPONSORING / MONITORING AGENCY NAME(S) AND ADDRESS(ES)
N/A

10. SPONSORING / MONITORING AGENCY REPORT NUMBER

11. SUPPLEMENTARY NOTES The views expressed in this thesis are those of the author and do not reflect the official policy or position of the Department of Defense or the U.S. Government.

12a. DISTRIBUTION / AVAILABILITY STATEMENT
Approved for public release. Distribution is unlimited.

12b. DISTRIBUTION CODE
A

13. ABSTRACT (maximum 200 words)

Body armor for military applications uses a composite system incorporating a monolithic ceramic front face plate backed by an Ultra High Molecular Weight Polyethylene (UHMWPE) textile system that offers a high mass efficiency. Issues with the current system include mobility, fracture and multi-hit performance degradation. It has been demonstrated that ceramic spheres have a higher mass efficiency as compared to monolithic ceramic tiles when applied against 3/8" chromium steel projectiles and 0.30 caliber M2AP projectiles. Within this study, the penetration resistance performance of two selected projectiles (AK-47 and M80) were studied against multiple front face ceramic armor systems. The back face deflection was measured using high-speed video to determine both in-plane and out-of-plane propagation. This data was correlated with load cell force measurements to provide a means to measure penetration resistance performance through determination of the work performed by the 80-layer UHMWPE backing with the selected front face ceramic systems. This work will enable a higher level of performance fidelity and enable optimized front face ceramic armor systems.

14. SUBJECT TERMS
body armor, ceramic spheres, monolithic ceramic, ceramic plates, Ultra High Molecular Weight Polyethylene, UHMWPE, Zylon, rifled projectiles, penetration resistance

15. NUMBER OF PAGES
109

16. PRICE CODE

17. SECURITY CLASSIFICATION OF REPORT	**18. SECURITY CLASSIFICATION OF THIS PAGE**	**19. SECURITY CLASSIFICATION OF ABSTRACT**	**20. LIMITATION OF ABSTRACT**
Unclassified	Unclassified	Unclassified	UU

NSN 7540-01-280-5500

Standard Form 298 (Rev. 2-89)
Prescribed by ANSI Std. 239-18

THIS PAGE INTENTIONALLY LEFT BLANK

Approved for public release. Distribution is unlimited.

INVESTIGATION OF ULTRA HIGH MOLECULAR WEIGHT POLYETHYLENE (UHMWPE) TEXTILE BACKING SYSTEMS INTEGRATED WITH CERAMIC SPHERE BODY ARMOR SYSTEMS

Brent W. Morrison
Lieutenant, United States Navy
BS, North Carolina State University at Raleigh, 2015

Submitted in partial fulfillment of the
requirements for the degree of

MASTER OF SCIENCE IN APPLIED PHYSICS

from the

NAVAL POSTGRADUATE SCHOOL
December 2021

Approved by: Raymond M. Gamache
Advisor

Abram H. Clark IV
Second Reader

Joseph P. Hooper
Chair, Department of Physics

THIS PAGE INTENTIONALLY LEFT BLANK

ABSTRACT

Body armor for military applications uses a composite system incorporating a monolithic ceramic front face plate backed by an Ultra High Molecular Weight Polyethylene (UHMWPE) textile system that offers a high mass efficiency. Issues with the current system include mobility, fracture and multi-hit performance degradation. It has been demonstrated that ceramic spheres have a higher mass efficiency as compared to monolithic ceramic tiles when applied against 3/8" chromium steel projectiles and 0.30 caliber M2AP projectiles. Within this study, the penetration resistance performance of two selected projectiles (AK-47 and M80) were studied against multiple front face ceramic armor systems. The back face deflection was measured using high-speed video to determine both in-plane and out-of-plane propagation. This data was correlated with load cell force measurements to provide a means to measure penetration resistance performance through determination of the work performed by the 80-layer UHMWPE backing with the selected front face ceramic systems. This work will enable a higher level of performance fidelity and enable optimized front face ceramic armor systems.

THIS PAGE INTENTIONALLY LEFT BLANK

TABLE OF CONTENTS

LIST OF FIGURES

THIS PAGE INTENTIONALLY LEFT BLANK

LIST OF TABLES

THIS PAGE INTENTIONALLY LEFT BLANK

LIST OF ACRONYMS AND ABBREVIATIONS

DOD	Department of Defense
DIC	Digital Image Correlation
ESAPI	enhanced small arms protective insert
fps	feet per second
HAP	hard armor plate
J	Joules
M80	7.62x51mm round (NIJ Level III)
m/s	meters/second
Mfps	million frames per second
MS/s	million samples per second
NATO	North Atlantic Treaty Organization
NIJ	National Institute of Justice
NPS	Naval Postgraduate School
PASGT	Personal Armor System for Ground Troops
psi	pound-force per square inch
SAPI	Small Arms Protective Insert
SI	Système international d'unités
TEMA	TrackEye Motion Analysis
UHMWPE	Ultra-High Molecular Weight Polyethylene
U.S.	United States

THIS PAGE INTENTIONALLY LEFT BLANK

ACKNOWLEDGMENTS

I would like to first thank Dr. Ray Gamache for his hard work and dedication throughout the thesis process. We were able to conduct insightful testing and analysis despite many setbacks, and he ultimately helped me deliver a well-thought-out thesis topic. I would also like to thank my wife, Amber, my daughter, Riley, and the rest of my family and friends for their support, encouragement, and sacrifices in time spent to allow me to focus on this research effort.

THIS PAGE INTENTIONALLY LEFT BLANK

I. INTRODUCTION

Within the early 2000s, a design shift within body armor systems occurred where monolithic textile armor systems were replaced with heterogeneous plate insert systems. The forward-facing strike surface being that of a monolithic ceramic plate backed by a textile armor system. The purpose of the ceramic plate is to reduce the incident pressure of the incident projectile through both reduction of the incident velocity and deformation of the sharp front ogive of the incident projectile. The textile armor system is then constructed to stop the decelerated/deformed projectile. This thesis effort will study the relationship of front face ceramic systems and the effect on the loading within the textile armor system.

Previous thesis research has shown promise with advancements in the replacement of monolithic ceramic armor systems with ceramic sphere systems. Ceramic sphere systems support the reduction in both mishandling damage and impact radius damage propagation as well as increasing flexibility [1]. Though there are many advantages to the replacement of a single monolithic plate with ceramic sphere system, the effectiveness of ceramic spheres compared to monolithic ceramic plates will be studied within this thesis [1].

To understand the loading that occurs from the ballistic impact, within each of the front face ceramic systems, unidirectional laminate layers of Ultra High Molecular Weight Polyethylene (UHMWPE) were constructed and mounted within a load cell system. Both instantaneous load cell and back face deflection measurements will be performed to quantify variations in physical stresses for both varied front face systems and incident projectiles.

The load cells will allow for determination of impact forces and how they dissipate over time. To measure the deflection, a high-speed video camera will track rear facing deformation enabling a better understanding of the type of loading variations that occur between different front face armor systems.

Analysis and comparison of the measured data within each impact experiment will enable quantitative comparisons of each ballistic impact propagation and correlated to

varying ceramic front faces. This ability will support the determination of the feasibility related to front face ceramic sphere applications.

II. BACKGROUND

A. MODERN BODY ARMOR HISTORY

Throughout history, as the enemy threat has advanced, so have the advancements in protection systems. Figure 1 shows the comparison of military casualties from both World Wars showing an approximate 200% increase in casualties. The rise in casualty-initiated efforts to redesign existing body armor systems during mid-WWII by the year 1942. The initial design incorporated metal plates sewn into a thick, cumbersome Nylon vest commonly referred to as a Flak Jacket [2]. This design only remains in use by the U.S. Navy for shipboard use.

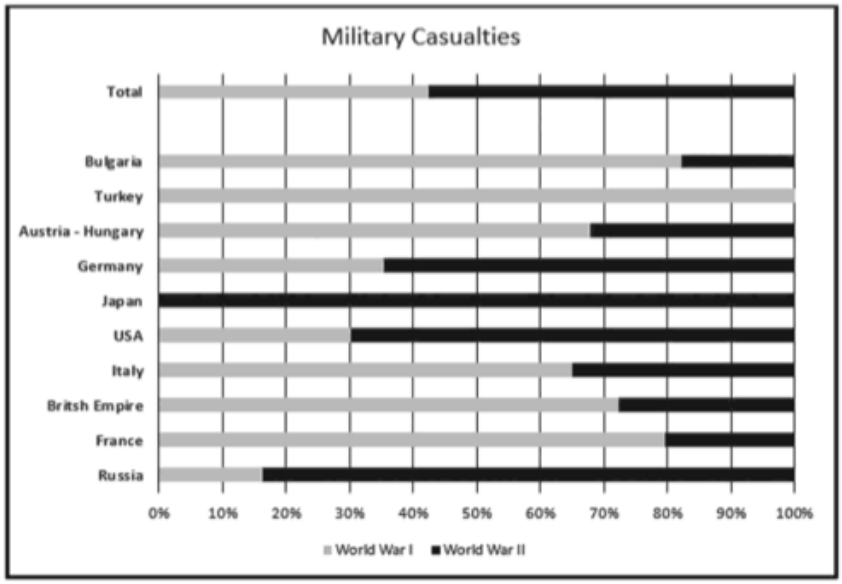

Figure 1. World War I Military Casualties Compared to World War II Military Casualties. Source:[2].

Post WWII, the Korean and Vietnam wars required a need for a less bulky and heavy design. Innovations in textile technology enabled lower weight high flexibility materials to defeat hemispherical nose projectiles and fragmentation but was ineffective in defeating close range sharp ogive rifled projectiles.

Doron, a fiberglass and plastic combination, was used for this initial application. However, by the year 1983 the Personal Armor System for Ground Troops (PASGT) was developed incorporating Kevlar as a replacement to Doron [3]. This was a revolutionary lightweight design that offered superior stopping power for the time.

PASGT was replaced in the early 2000s by the Interceptor Body Armor [4]. The interceptor body armor consisted of a Kevlar internal liner and four pocket systems to enable armor plate inserts. The insert plates enabled enhanced protection against rifled threats protecting both front and back regions of the torso as well as specific side regions lower on the torso. The insert protective plates are referred to as either Small-Arms Proactive Inserts (SAPI) or Enhanced Small-Arms Proactive Inserts (ESAPI) [4]. Each SAPI or ESAPI plate is constructed as a heterogeneous system of two layers. The front facing plate is a monolithic ceramic plate followed by a UHMWPE textile armor backing system. This plate has one of the highest mass efficiencies, and it continues to be fielded today.

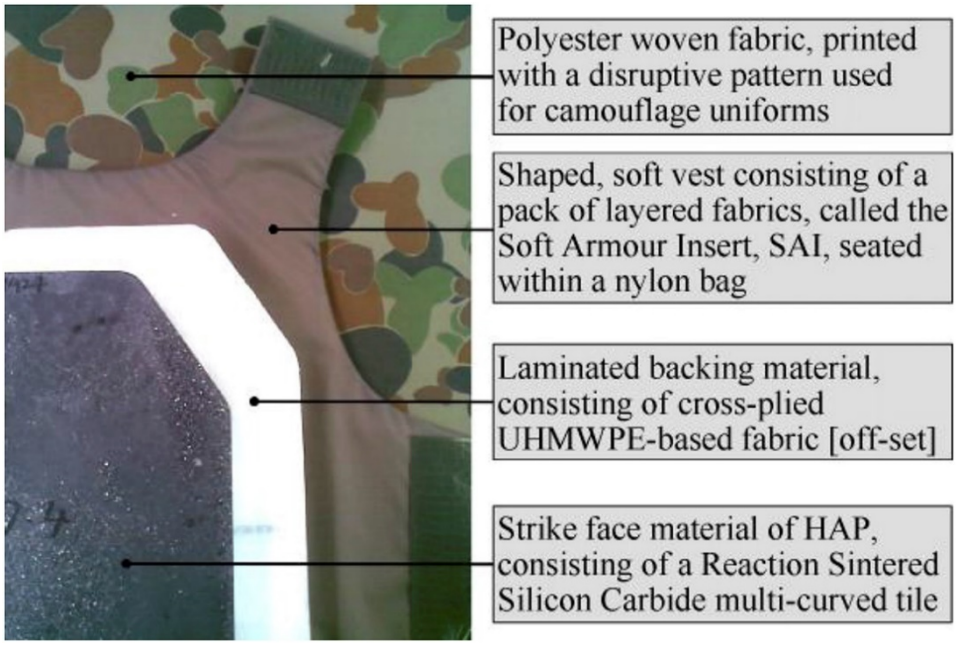

Figure 2. Modern Body Armor Composition with SAPI/ESAPI Style Plate. Source: [1].

B. BODY ARMOR STANDARDS

The Department of Justice has been responsible for developing a series of standards for body armor performance. The document developed by the National Institute of Justice (NIJ) is Standard-0101.06 [5].

1. ARMOR LEVELS

NIJ standards are divided into levels of protection, as presented in Figure 3. Current SAPI and ESAPI plates, are rated at NIJ Level III and Level IV respectively [6]. The primary focus for this thesis is Level III threats. Within this thesis, both M80 (NIJ Level III) and AK-47 projectiles will be studied against composite armor systems.

	Test Variables					Performance Requirements			Shot Requirements					
Armor Type	Test Round	Test Bullet	Bullet Mass	Conditioned Armor Test Velocity*	New Armor Test Velocity*	Hits Per Panel at 0° Angle	Maximum BFS Depth	Hits Per Panel at 30° or 45° Angle†	Shots Per Panel	Panel Size	Panel Condition	Panels Required	Shots Required	Total Shots Required
IIA	1	9 mm FMJ RN	8.0 g (124 gr)	355 m/s (1165 ft/s)	373 m/s (1225 ft/s)	4	44 mm (1.73 in)	2	6	Large	New	4	24	144
											Conditioned	2	12	
										Small	New	4	24	
											Conditioned	2	12	
	2	.40 S&W FMJ	11.7 g (180 gr)	325 m/s (1065 ft/s)	352 m/s (1155 ft/s)	4	44 mm (1.73 in)	2	6	Large	New	4	24	
											Conditioned	2	12	
										Small	New	4	24	
											Conditioned	2	12	
II	1	9 mm FMJ RN	8.0 g (124 gr)	379 m/s (1245 ft/s)	398 m/s (1305 ft/s)	4	44 mm (1.73 in)	2	6	Large	New	4	24	144
											Conditioned	2	12	
										Small	New	4	24	
											Conditioned	2	12	
	2	.357 Magnum JSP	10.2 g (158 gr)	408 m/s (1340 ft/s)	436 m/s (1430 ft/s)	4	44 mm (1.73 in)	2	6	Large	New	4	24	
											Conditioned	2	12	
										Small	New	4	24	
											Conditioned	2	12	
IIIA	1	.357 SIG FMJ FN	8.1 g (125 gr)	430 m/s (1410 ft/s)	448 m/s (1470 ft/s)	4	44 mm (1.73 in)	2	6	Large	New	4	24	144
											Conditioned	2	12	
										Small	New	4	24	
											Conditioned	2	12	
	2	.44 Magnum SJHP	15.6 g (240 gr)	408 m/s (1340 ft/s)	436 m/s (1430 ft/s)	4	44 mm (1.73 in)	2	6	Large	New	4	24	
											Conditioned	2	12	
										Small	New	4	24	
											Conditioned	2	12	
III	1	7.62 mm NATO FMJ	9.6 g (147 gr)	847 m/s (2780 ft/s)	-	6	44 mm (1.73 in)	0	6	All	Conditioned	4	24	24
IV	1	.30 Caliber M2 AP	10.8 g (166 gr)	878 m/s (2880 ft/s)	-	1 to 6	44 mm (1.73 in)	0	1 to 6	All	Conditioned	4 to 24	24	24
Special	-	Each test threat to be specified by armor manufacturer or procuring organization.				Armor performance and shot requirements shall depend on armor type.								

*Target measurement velocity. Fair hit measurement velocities must be within ± 9.1 m/s (± 30 ft/s) of this value, as defined in Section 7.6.
†Each armor that is to be shot at angles other than 0° shall be shot once at a 30° angle and once at a 45° angle.

Figure 3. NIJ Test Performance Standards. Source: [5].

2. PROJECTILES OF INTEREST

Both NIJ Level III threats (7.62x51mm M-80) and AK-47 (7.62x39mm) ball round shown in Figure 4 will be considered within this thesis.

Figure 4. (Left) 7.62 x 51mm NATO (M80). (Right) 7.62 x 39 mm (Standard AK-47 Round) Source:[7].

The M80 round is a 147 grain (9.6 g) full metal jacket projectile with a soft lead alloy core traveling at approximately 847 ± 9.1 m/s [5]. This is equivalent to an approximated kinetic muzzle energy of 3370-3518 Joules. Its use for NIJ testing was due to its popularity of use in many U.S. military arms since the 1950s, including the M240B machine gun as well as several others.

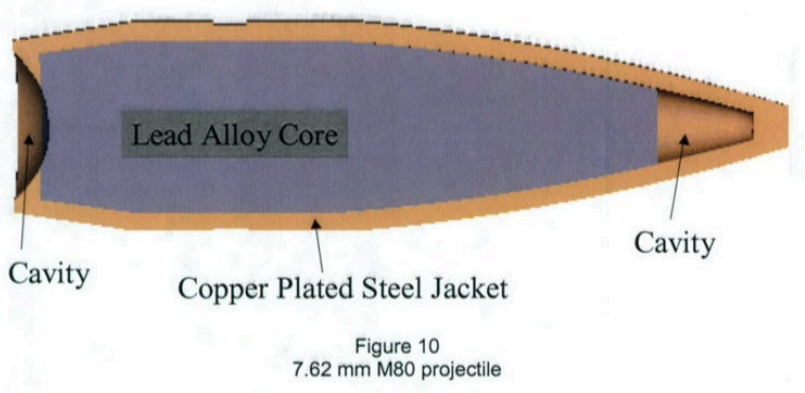

Figure 5. 7.62 x 51mm NATO (M80) Cross-Section. Source:[8].

The AK-47 ball 7.62 x 39 mm is a very critical round to defeat due to its devastation of U.S. military personnel in the field. This is due to the sheer production number of AK-47s and variants throughout the world which totals to approximately 100-150 million making it the world's largest production small arm in history [9]. The large distribution and low cost of this rifle make it common amongst all adversaries especially those in the Middle East. This round is a FMJ with a solid steel core. The muzzle velocity of the AK-47 ball round is approximately 738 m/s ± 9.1 m/s which generates a kinetic muzzle energy of 2125-2232 Joules [10].

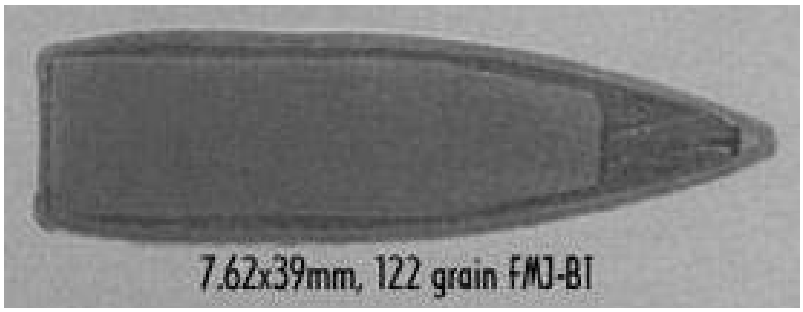

Figure 6. 7.62 x 39 mm (Standard AK-47 Round) Cross-Section. Source:[11].

The muzzle energy for the M80 is significantly higher than that of the standard AK-47 round. This would imply that if it meets NIJ Level III standards that the 7.62 x 39 mm round would not require testing; however, this is not the case as this round has been

known to defeat armor regardless [12]. This is primarily due to the core of the round itself. The steel core of the 7.62 x 39 mm does not deform as much as that of the M80 lead alloy core. This will be discussed further in the next section [12].

C. CURRENT TWO-PIECE ARMOR SYSTEMS

Current operational body armor systems for the U.S. military use either SAPI or ESAPI plates. Each plate consists of a monolithic (formed of a single larger piece) of ceramic followed by multiple compressed layers of UHMWPE. As mentioned previously the front face armor system enables both a reduction in incident velocity and blunting/breakup of the incident projectile enabling a reduction in pressure to the textile armor backing system. Figure 7 presents a basic simulation of an incident round impacting a SAPI plate armor system.

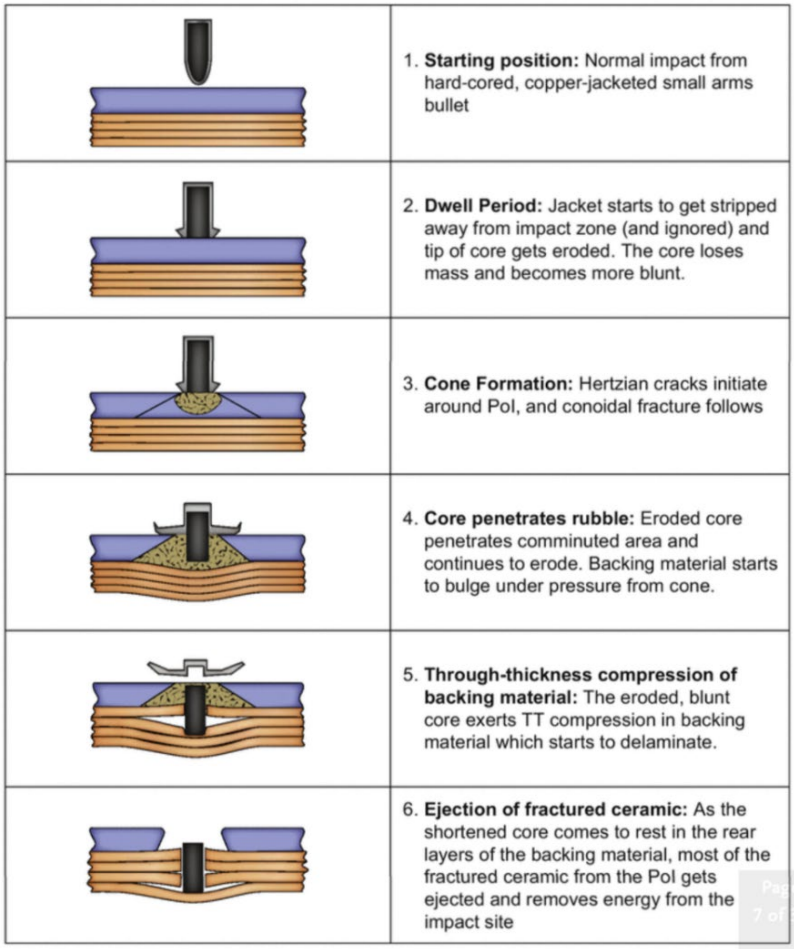

Figure 7. Projectile Reaction against a SAPI-Style Plate. Source:[13].

1. CERAMIC STRIKE FACE

This monolithic strike face layer serves a dual function of quickly decelerating the incident projectile while also deforming or blunting the projectile as much as possible making it easier for the UHWPE to stop the projectile and any debris. From Figure 7 above, we can see the progression of the round through the ceramic plane [13]. The first major blunting of the projectile during the dwell time of the round. This is where the copper jacket it ripped backwards as the projectile makes contact, and the cavity located directly at the tip of the core is exposed [13]. As the core contacts the ceramic, it begins to blunt and produce a mushroom effect an effect of ballistic impact where the copper jacket of the projectile is rolled back to expose the inner core that contains the majority of the kinetic

energy to inflict the most damage. This interaction severely cracks the ceramic plate and even pulverizes the immediate area into a fine ceramic dust, and this is described as the cone formation as seen above [13]. This core continues to blunt, decelerate, and partially erode throughout the thickness of the ceramic while simultaneously beginning to deform the textile backing into a tent-shape wave. This continues until the leading edge breeches the back of the ceramic. At this time, a handover is established to the textile backing where the blunted core cuts through layers until reaching a final resting place within the fibers. More on this description later.

The three ceramics in use for most modern two-layer systems are alumina (Al_2O_3), silicon carbide (SiC), and boron carbide (B_4C) with a thickness of 0.270 ± 0.02 inches; listed below in Table 1 are metrics for these ceramics [1]. SiC is by far the most common in use today, so for the scope of this thesis when using monolithic ceramic plates, SiC will be the tiles used.

Table 1. Mechanical Properties of Ceramics. Source: [1].

Ceramics			
	Alumina (Al_2O_3)	Silicon Carbide (SiC)	Boron Carbide (B_4C)
Density [g/cc]	3.9	3.21	2.51
Hardness Knoop [kg/mm^2]	14.1	26	31
Flexural Strength [MPa]	338 - 379	480	410
Compressive Strength [MPa]	2600	3500	3900
Hugoniot Elastic Limit [GPa]	6.71	15-16	18-20
Cost	Low	Medium	High

The biggest drawback to using monolithic ceramic plates is that they are prone to cracking under accidental impact from dropping or even the generating of micro-cracks as

the plate is used daily. As the monolithic plate is formed of a single large piece of ceramic, any type of drop to include impact on the corners, impact of the strike face itself, or even improper storage allowing for contact between sets of plates and other hard surfaces could cause these initial cracks that greatly inhibit the armor's first strike mitigation capabilities [1]. Past thesis efforts focused on the exploitation of ceramic geometry (ceramic spheres) to address this tendency to crack [1]. The solution was to create a lattice of hexagonally-close-packed (hcp) spheres, such as in Figure 8. This concept would limit crack propagation as a result of negligent handling that could extend the entire length or width of the panel to just a few small spheres at the impact sight or even no damage at all.

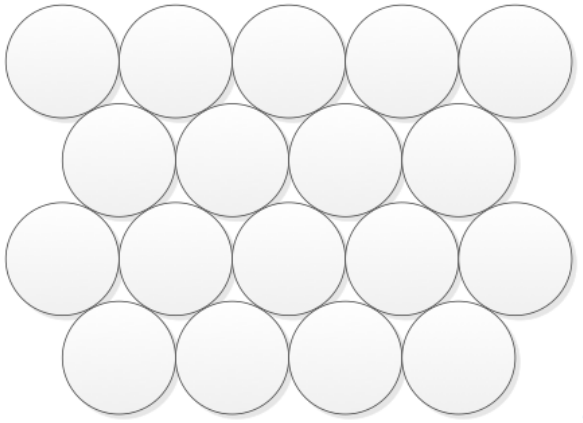

Figure 8. Hexagonal-Close-Packed Structure of Ceramic Spheres Used in Past Thesis Work. Source: [1].

In addition to the study of ceramic spheres with a simple binding agent, past thesis efforts also studied the effect of encapsulation for the ceramic spheres. This essentially creates a semi-solid panel from the spheres by heating an encasing agent to a liquid state, adding it around the spheres in a mold, and allow the agent to cure [1]. There was promise seen with two of these encapsulating agents: the Versalink P-1000 polyurethane additive, which is a product of the Bayville Chemical Supply Company Inc., and an in-house created Aluminum 319 (A319) encapsulating agent with T-6 tempering [1],[14]. These encapsulated targets will be analyzed for the purpose of this thesis as well.

2. POLYMER REAR PANEL

The current SAPI rear panels are constructed of multiple uniaxially aligned UHMWPE fibers in a crosshatch pattern that follows the orientation seen in Figure 9 with each elongated cylinder representing a UHMWPE fiber lengthwise and each circle representing the cut end of the UHMWPE fiber. Each single layer of UHMWPE consists of 4 layers or plies of fibers. Figure 9 is representative of approximately 4 layers where 2 layers are in the 0-degree orientation and 2 layers are in the 90-degree orientation forming a total thickness of approximately 16 UHMWPE fibers. This pattern is repeated to form the 35-40 layers required for modern SAPI plates [1].

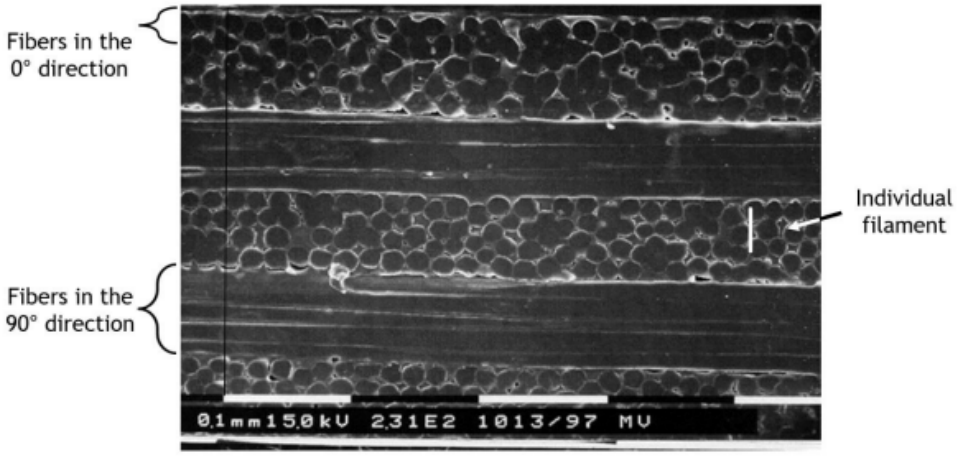

Figure 9. UHMWPE Fiber Orientation. Source: [15].

However, to understand what is happening as a projectile initially contacts a single fiber at that scale, it is necessary to analyze what is happening to a single fiber under a rapid impact load test. Upon impact, a fiber will immediately begin to experience a transverse wave in the direction of the velocity vector of the projectile, which will be referred to as the transverse wave front [15],[16],[17]. Smith displays this analytically in Figure 10 in his research [16]. For his analysis in this figure, the rapid impact force, which for the purpose of this thesis is the incident projectile, is approaching a single fiber from below and creating the tenting effect observed where the bolded line represents the present waveform and the dashed line as the same waveform after a delta time (dt or Δt) [16]. The

transverse wave height propagates at a speed V in m/s for a distance of Vdt for any given Δt after impact. Concurrently, the outward propagation of the transverse wave perpendicular to the impact has velocity U in m/s for a distance equal to $Ut(1+\in_2)cos\theta$ for any given Δt after impact where $\in_2$is the strain of the material towards the maximum height of the tent formed and theta is the angle formed by the propagation of the tent [16].

In advance of this transverse wave, that propagates in the plane of the target, a region is created where the material is pulled inwards toward the point of impact, i.e.,. from point Q to Q* in Figure 10 [15]. This strain wave is referred to as the Longitudinal Wave Front or the Elastic Wave Front and experiences strain $\in_p$outboard of the impact sight [15],[16],[17]. Smith concluded that for a single fiber under rapid impact loading that tensions T_2 and T_p could be solved for given observation of deformation values, and that for most cases the tensions and strains are equivalent [16]. Analysis of these trends with different material properties provide a basis for the study of polymer body armor for the purpose of this thesis though no testing was conducted by Smith against multiple layers of fibers or orientations of the fibers when compiled together. Deriving a similar comparison for analysis as a function of layer number and orientation could pave the way for better body armor optimization.

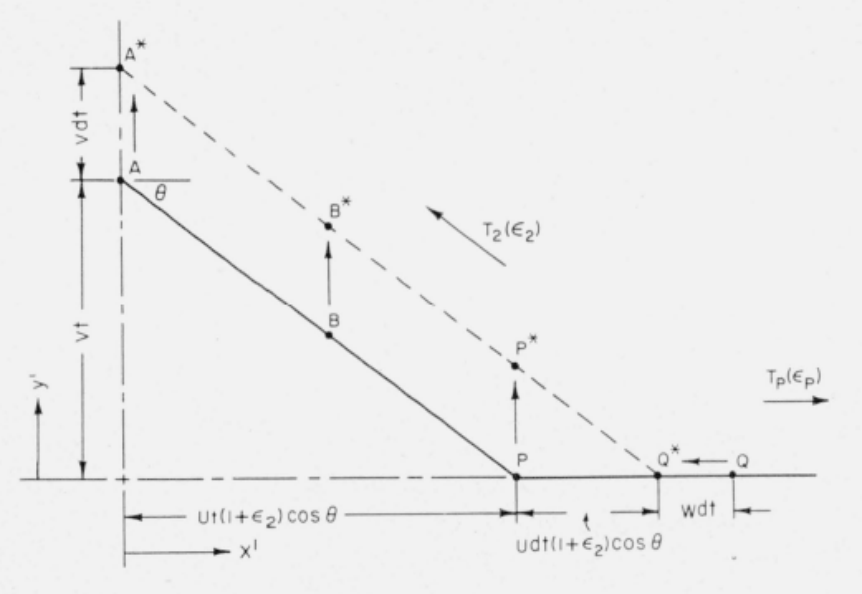

Figure 10. Single Fiber Under Rapid Impact Loading From a Projectile. Source: [16].

Understanding these physical traits has allowed for better mass efficiency by studying material properties and construction techniques such as the cross hatch pattern discussed before [15]. This is utilized in current SAPI and ESAPI plates by combining specifically cut torso-shaped layers ensuring that each layer is exactly 90° in orientation from the preceding layer. The layers are then heated to an adhesion temperature in which they can be pressed together but still retain their uniaxial shape for each individual fiber. This allows the fibers to retain their elastic and plastic wave front capabilities necessary for stopping projectiles. After curing to its final form, it can be encased in a weatherproofing material and utilized as the second piece of the composite body armor system; this finalized construction can be seen in Figure 11.

Figure 11. UHMWPE Plate. Source: [18].

D. THESIS ORGANIZATION AND RESEARCH QUESTIONS

This thesis attempts to analyze the combination of several previously researched ceramic interfaces and a heavy UHMWPE textile during rapid impact testing. Analysis will be completed on the textile layer by using load cells in combination with a light gas gun to

record residual forces after the round has penetrated each ceramic front panel. A high-speed camera will also be used to track deformation and analyze the elastic and plastic waves generated on the textile backing as function of time.

This thesis will include 5 chapters: I. Introduction, II. Background, III. Experimental Setup and Data, IV. Data Analysis, and V. Conclusion. Chapter I discusses the purpose and justification for attempting this data collection and analysis. Chapter II discusses a general background for modern body armor that includes: a brief history on body armor evolution, a discussion of body armor standards to include NIJ standards as well as projectiles of interest, and an overview of the current ceramic/textile two-layer body armor system currently in use.

Chapter III discusses an experimental setup that details the creation of the ceramic and UHMWPE targets as well as the combinations that were established for tests. It explains the lab equipment and setup associated with the operation of the light gas gun to include the program used, the parameter descriptions for the gun, the sample mounting and setup, and the high-speed camera setup. Chapter IV discusses the load cell data in order to determine the forces on the UHMWPE backing as a function of time after impact as well as describes the use of TEMA to track back face deformation and record the elastic/plastic wave propagation as a function of time. Chapter IV is an analysis of the collected data from Chapter IV. Chapter V presents a conclusion with recommendations for follow-on research.

THIS PAGE INTENTIONALLY LEFT BLANK

III. EXPERIMENTAL SETUP

A. TEST MATRIX

Within this thesis, uniaxial 4-filament layered UHMWPE strips were used to construct an 80-layer fiber armor. This fiber system was tested as a back face system incorporating a selected front face ceramic system including: a SiC tile, 90 and 99.5 % alumina (AD90 and AD995, respectively) ceramic sphere lattices, an aluminum encased lattice of AD90 spheres, and a P1000 encased lattice of AD90 spheres. The aforementioned targets listed were engaged with both the 7.62 x 39 mm AK-47 and 7.62 x 51 mm M80 projectiles as described in Table 2.

Table 2. Test Matrix for Experiment

Shot #	Target Description (Ceramic Front Face)	Target Description (Polymer Backing)	Projectile/ Weight	Breech Pressure (psi)	Sample Rate (FPS)
1	SiC 7.2 x 7.2 cm tile 0.635 cm thickness	80-Layer UHMWPE	AK-47 Ball 7.62 x 39 mm/ 7.835 g	4000	206,349.2115
2	Al_2O_3 AD995 7.62 x 7.62 cm 4 Row 0.953 cm thickness	80-Layer UHMWPE	AK-47 Ball 7.62 x 39 mm 7.854 g	4000	206,349.2115
3	Al_2O_3 AD90 7.62 x 7.62 cm 4 Row 0.953 cm thickness	80-Layer UHMWPE	AK-47 Ball 7.62 x 39 mm/ 8.017 g	4000	206,349.2115
4	Al Encapsulated Al_2O_3 AD90 0.953 cm thickness	80-Layer UHMWPE	AK-47 Ball 7.62 x 39 mm/ 7.987 g	4000	206,349.2115
5	P1000 Encapsulated Al_2O_3 AD90 0.953 cm thickness	80-Layer UHMWPE	AK-47 Ball 7.62 x 39 mm/ 7.843 g	4000	206,349.2115
6	Al_2O_3 AD90 7.62 x 7.62 cm 4 Row 0.953 cm thickness	80-Layer UHMWPE	M80 Ball 7.62 x 51 mm 9.586 g	4000	153,664.3064
7	SiC 7.2 x 7.2 cm tile 0.635 cm thickness	80-Layer UHMWPE	M80 Ball 7.62 x 51 mm 9.575 g	4000	153,664.3064

B. CERAMIC TARGET VARIANTS AND CREATION

To compare the performance of the ceramic sphere systems, a 0.635 cm SiC tile was studied as a comparison to the ceramic sphere systems. Tiles studied had aerial

dimensions of 7.62 x 7.62 cm with a thickness of 0.65 cm. Figure 12 presents the SiC tile with the 80-layer UHMWPE backing. Adhesion of the front face ceramic systems was performed using an epoxy.

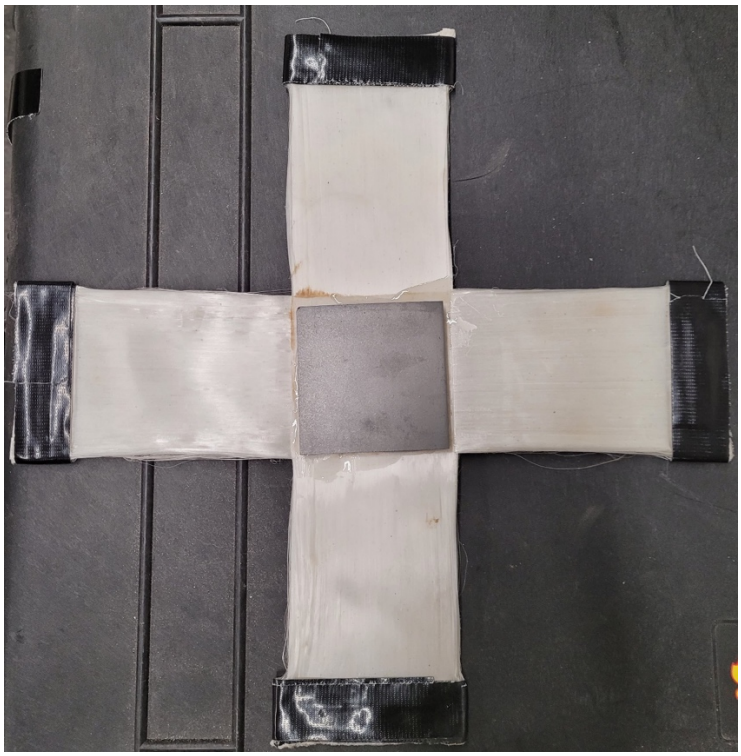

Figure 12. SiC Tile Attached to 80-Layer UHMWPE Sample

The remaining tests incorporated 0.9525 cm ceramic spheres in both a polyurea/aluminum encapsulation and with no encapsulation (thin adhesive).

An aluminum encapsulation was studied in Shot 4. The encapsulation was performed in house using Al A319 Alloy and T6 tempered [1]. The thickness of the aluminum encapsulated spheres is pressed to the same thickness of the spheres themselves at 0.9525 cm.

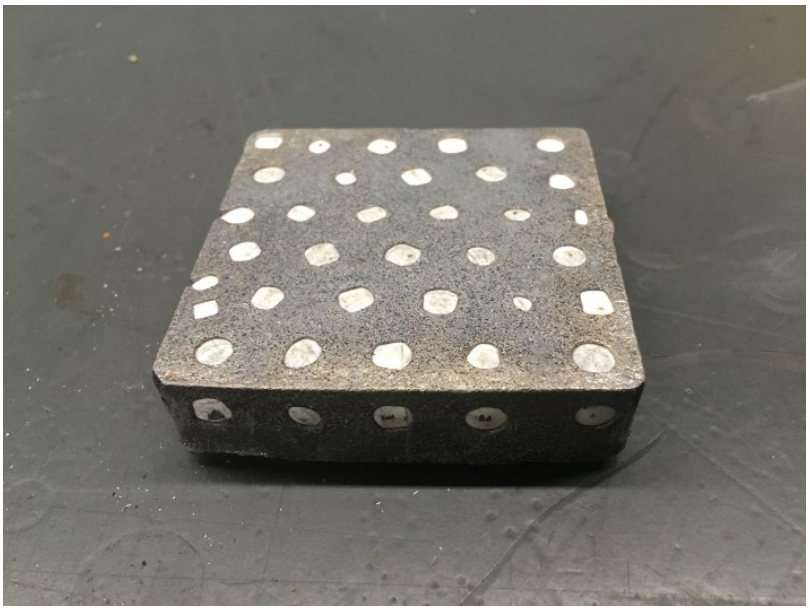

Figure 13. T6 Tempered A319 Aluminum Alloy Encapsulate 3/8” Ceramic Spheres

Shot 5 utilized a Versalink P1000 polyurea to encapsulate the AD90 ceramic spheres. The P1000 is a two-part mix of an amine and isocyanate at a ratio of 4:1 amine to isocyanate [14]. The combination was also kept to a thickness of 0.9525 cm for proper comparison. P1000 was selected based on its tensile strength (> 34.5 MPa) and high elongation (> 300%).

Figure 14. Versalink P1000 Encapsulate 3/8” Ceramic Spheres

C. UHMWPE BACKING SYSTEM

The Dyneema HB26 UHMWPE backing system incorporated in all target systems was un-pressed uni-axial four filament thick strips having dimensions of 7.62 cm x 38.1 cm [19]. After assembly of the 80 layers the material was heated and pressed to 3000 psi.

1. Mount and Assembly

To enable optimized penetration resistance performance of the HB26 material, it must be formed into multiple layers and hot pressed. To assemble the UHMWPE target, a custom jig was fabricated (Figure 15) enabling both proper alignment and providing a surface area to press the center 7.62 cm x 7.62 cm region. Nolax A21.2007 adhesive laminate material was cut to ~ 1.3 cm by 5 cm sections and placed between each internal layer, at the end locations, to adhere the layers when clamped for the ballistic testing. Thin Teflon strips were placed on the exterior end regions of the material before securing within the end clamps to reduce any adhering of the sample to the mount due to the Nolax adhesive extruding during the heating process.

Figure 15. Custom Jig for UHMWPE with Sample Mounted. Source: [15]

2. Furnace

A furnace was used to heat the fiber systems prior to pressing. The jig assembly including the UHMWPE and pressing block were placed in the furnace at 135 °C for three hours.

Figure 16. Thermal Product Solutions Tenny Furnace

3. Pressing

A 75-ton hydraulic press was used to press the UHMWPE fabric to 3000 psi. Upon completion of heating, the jig and pressing block were immediately transferred to the press. The jig was then centered, and the pressing block was aligned on the center of the fiber system. The entire mount system was then placed under a 13.5-ton load for 15 minutes while the clamps at each end were continually tightened to both promote adhesion of the Nolax film to the UHMWPE and initiate a corrugation on the target ends to ensure no slippage will occur.

Figure 17. Baileigh 75 Ton Air/Manual Hydraulic Shop Press

D. PROJECTILE CONSTRUCTION

Both AK-47 Ball (7.62 x 39 mm) and M80 (7.62 x 51 mm) projectiles were tested against the selected target systems. To launch the projectiles, from the light gas gun, a four-petal serrated sabot was incorporated to enable launching within the 2.54 cm smooth bore barrel. The sabot (Figure 18) is constructed from four solid 3D-printed polycarbonate serrated petals.

Figure 18. Cross-Section of Sabot with 7.62 x 39mm AK-47 Ball Projectile.

E. TEST SETUP

Ballistic testing was conducted at the Armor Development Lab (Bldg. 216), located within the Monterey Pines Golf Course. The testing equipment includes light gas gun, textile target system (with two load cells), high-speed video camera and 3D printed support material.

Figure 19. 1” Light Gas Gun. Source: [1].

1. Gas Gun System

The light gas gun incorporates a 2.54 cm diameter smooth-bore barrel with a total barrel length of 4 meters and a regenerative 42 MPa breech. The compressed dry air used, within the breech, is generated by a two-stage compressor system and stored in two double walled compressed air tanks. (Figures 20 and 21).

A catch tank system consisting of three sections is placed on the breech side of the light gas gun. The first section incorporates the laser velocimeter and enables the 1 m free flight to enable aerodynamic sabot separation. The middle tank incorporates both the sabot stripper and target holder system. The third and final section of the catch tank enables arrest of both the projectile and any residual fragmentation through a qty of 16 0.635 cm thick mild steel plates.

Figure 20. High Output Air Compressor. Source: [1].

Figure 21. Compressed Dry Air Storage Tanks. Source: [1].

A 1 MPa compressor in incorporated within the light gas gun system enabling both initial priming of the 6000 psi compressor as well as providing the air supply for all electro-pneumatic valves controlling the air flow for breech filling as well as gun firing of the light gas gun (Figure 22).

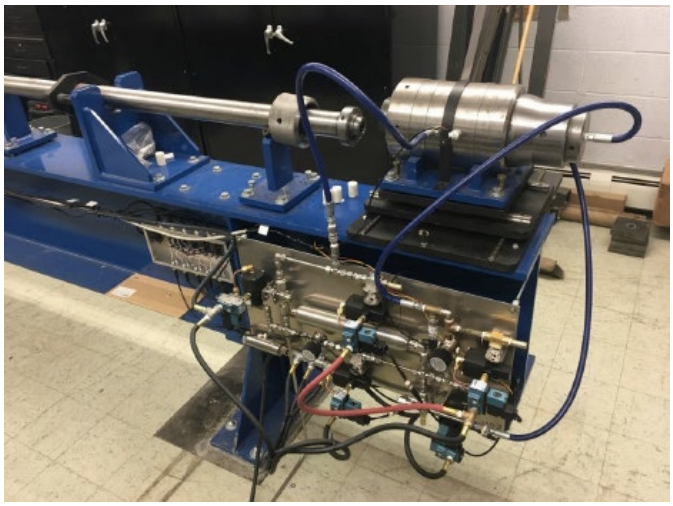

Figure 22. Light Gas Gun Breech and Pneumatic Actuators.

Separation of the sabot from the projectile requires a minimum flight distance, to enable the four-petal sabot to aerodynamically separate, of 1 m followed by a stripper plate. The stripper plate, placed 1 meter from the gun muzzle, within the middle tank incorporates a small hole large enough to enable the projectile to continue flight but too small for the sabot to pass through.

The target holder system is mounted in the final portion of the middle tank behind the sabot stripper plate. As viewing of the textile fibers is required during the ballistic impact, several layers of 5 cm thick clear polycarbonate material (plexiglass) were attached to contain any exiting debris while enabling direct viewing of the back face system.

Figure 23. Target, Camera, and Plexiglass Configuration.

Firing of the light gas gun is controlled by a LabVIEW software package, as seen in Figure 24. The software enables control of the breech filling, firing, and purging of the light gas gun after firing. The software control of the light gas gun is enabled through the direct control of five electro-pneumatic valves (Figure 22). Control and firing of the light gas gun are performed within the control room located in the lower entrance are to bldg. 216 (Figure 25).

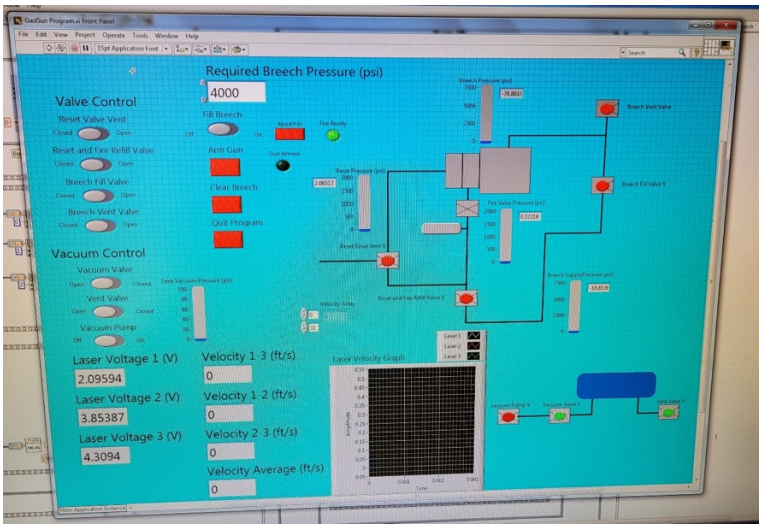

Figure 24. Labview Light Gas Gun Software Program (GUI)

Figure 25. Light Gas Gun Control Room. Source: [1].

2. Target Holder System and Data Collection

Assessing the loading of the textile armor systems utilized a custom fabricated mount enabling the placement of two load cells located in series to the two planar orthogonal axes (Figure 26). The load cells, Omega LCHD-1k [20], are positioned to gather perpendicular tensile load data along the X and Y axes of the target system.

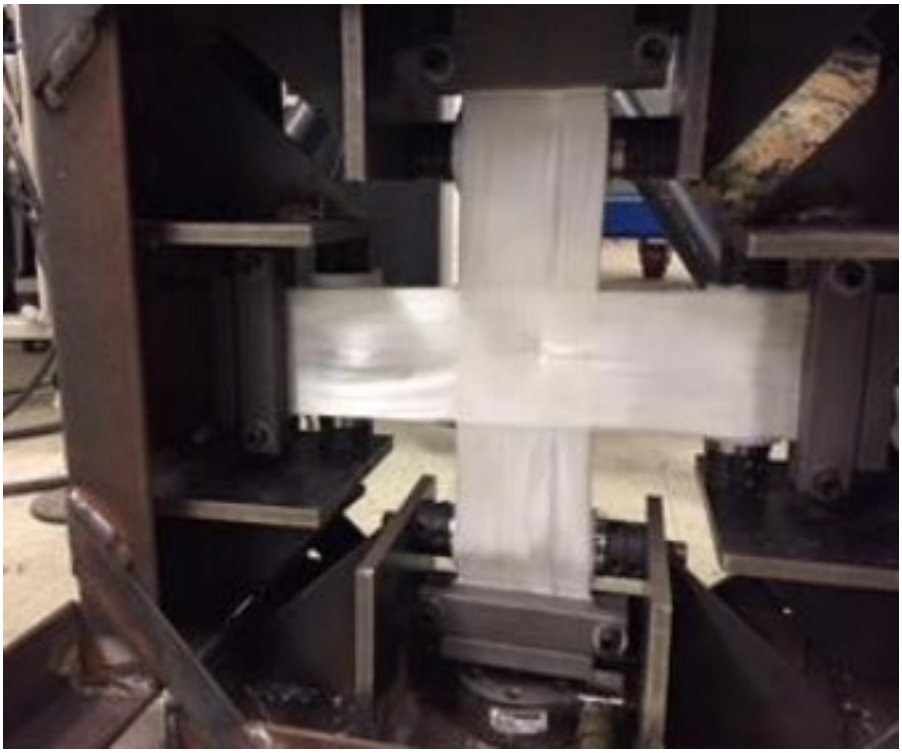

Figure 26. Testing Mount with Omega LCHD-1k Load Cells. Source: [15].

To measure the incident velocity, two break screens (Figure 27) were placed on the front side of the target with a separation distance of 8.25 cm. The break screens are constructed of a conductive material pattern covering a specific area with a uniform conductive path. When a projectile strikes the screen, the conductive path will be broken and an interfaced trigger box will generate a short time response pulse. A Whithner trigger box 1000 [21] interfaced to the break screen enables a 10V output signal when the conduction of the break screen is broken. Within all experiments the known distance between the two screens enables an accurate velocity measurement. In addition, the second screen, closest to the target, triggers both the high-speed video camera and the load cells.

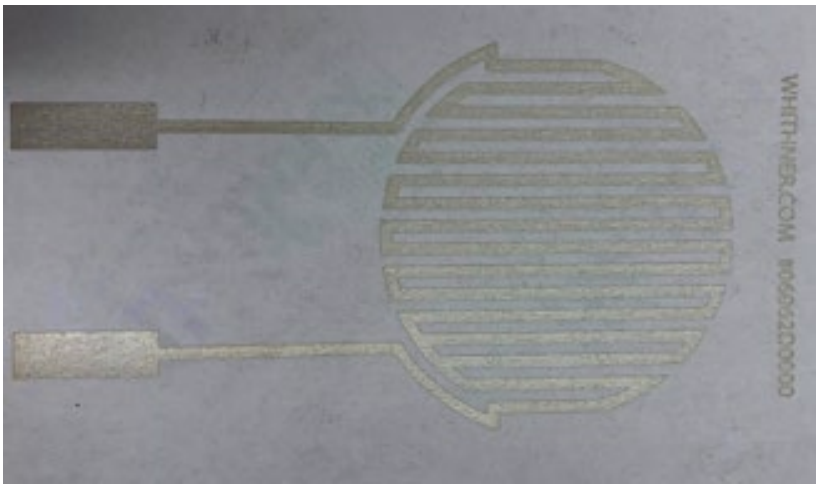

Figure 27. Whithner Silver Conducting Break Screens

Figure 28. Whithner EZ-Triggerbox 1000. Source: [1].

The signals generated from both break screens were sent to a Tektronix TDS 3034B Digital Oscilloscope. The measured time duration between break screens at a known distance provides a measurement for the incident velocity.

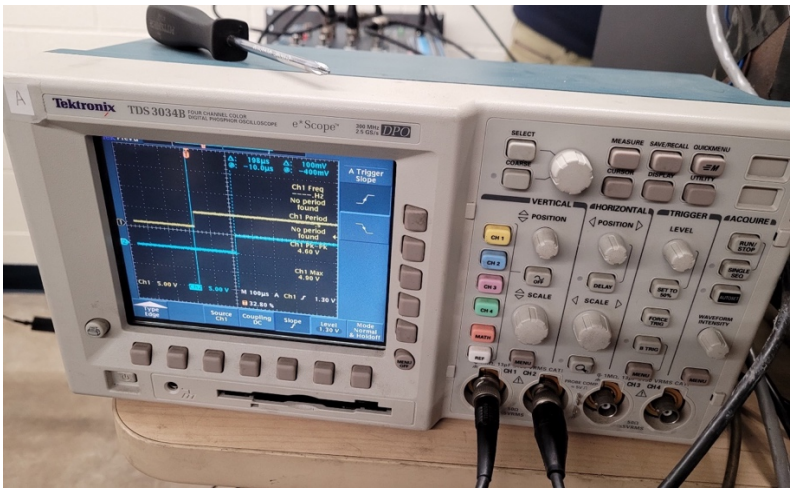

Figure 29. Tektronix TDS 3034B Digital Oscilloscope

The load cells and high-speed video are triggered from a pulse generator (Berkeley Nucleonics model 577) (22) that is initiated by the second break screen closest to the target. The pulse generator enables synchronization of the timing between the load cell and high-speed video camera.

Synchronization of the load cell is enabled using a Wheatstone bridge circuit (Figure 31) to time stamp the triggering of the high-speed video. The output of the bridge provides a voltage step which is received within the third load cell channel of the data acquisition card. This step rise

All load cell data is acquired within a National Instruments NI 9237 data acquisition card [23] using LabView software and stored directly within a laptop computer. The data acquisition for the NI 9237 is 24-bit resolution with a sampling rate of 50kHz.

Figure 30. Berkeley Nucleonics 577 Pulse Generator. Source: [15].

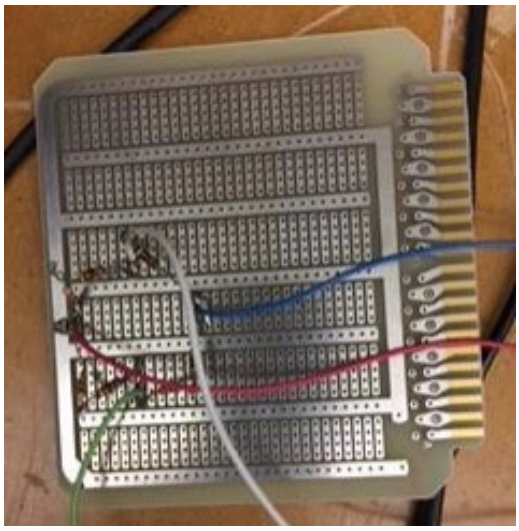

Figure 31. Wheatstone Bridge Circuit for Trigger on Load Cell Data Collection. Source: [15].

Figure 32. National Instruments NI 9237 Data Acquisition Card. Source: [15].

3. High Speed Camera

A Vision Research Phantom v2511 high speed video camera [24] capable of frame rates up to 1MFPS and image resolution up to 1280 x 800 pixels was used to image the back face deflection of the target systems. A Carl Zeiss 50mm lens was used to collect all target images.

Figure 33. Vision Research Phantom v2512 High-Speed Camera

The Phantom camera was positioned immediately behind the target section of interest as pictured in Figure 23 and perpendicular to the trajectory of the incident round.

Multiple panels of 5 cm thick clear plexiglass were placed between the sample and the camera for safety and camera protection.

A single high output light, Visual Instrumentation Corp. Model 901000H, was placed outside the plexiglass to illuminate the target section of interest.

Figure 34. Visual Instrumentation Corp. Model 901000H High Output Light

The imaging setup enables measurement of the back face deformation propagation of both the X and Y areal deflection as well as the vertical deflection along the Z axis. To enable observation of both areal and vertical deflection, 3D printed mirror systems were constructed to measure the Z axis deformation. One mount is labeled with markings for every $1/16^{th}$ inch from 0 to 2 inches along the Z axis. The opposing mount was constructed with a mirror placed at a 45-degree angle to provide the high-speed camera with a method for viewing the areal and perpendicular deflection simultaneously (Figure 35). The collected video is then processed using the TEMA 2D imaging program.

Figure 35. Testing Mount Configuration with Mirror and Measuring Block Installed

F. TEMA

The TEMA 2D tracking program provides the user with the ability to extract kinematic data such as position, velocity, and acceleration from video files. This capability will be used to track the back face deformation from a ballistic impact.

1. Transverse Wave Outward Propagation Data

Setup for the TEMA 2D tracker includes importing the video files and inputting the camera parameters. Measurements from video files require reference to a known distance for in-plane tracking. To accomplish this, two small black dots were marked on the back face of the sample prior to engagement and measured to a known distance of 7.62 cm. A distance measurement tool within the program was utilized to measure the distance from the determined center of impact to the leading edge of the outward wave for each frame until completion.

2. Transverse Wave Height Propagation Data

A similar approach was utilized to attain values for the height of the tent formation created by the transverse wave. Two tracking points were placed in the mirror frame of the target video utilizing the measuring block in the mirrored image. This distance was set to 3.81 cm from point to point for its corresponding values on the measuring block again ensuring the best gradient of the tracking points in relation to the background by altering settings for contrast, color, etc. Similar to the preceding section, the distance tool was used to manually measure the height of the tent formation from frame to frame. Results for height versus time for each sample were again recorded in Excel with the preceding data and indexed to their respective frame times.

G. WORK CALCULATIONS

Through measurement of both load cell tension and back face deflection measurements, the total work performed by the textile backing system can be calculated. Total tension, as mentioned earlier, is measured through the application of two load cells aligned along the X and Y axis. To determine the out-of-plane tension performing work on the incident projectile, the angle of the textile fabric out of plane must be determined. Measuring back face deflection, both in-plane and out-of-plane, enables the out of plane deflection angle calculation.

In addition to enabling the out-of-plane component of tension, the position change of the back face correlated to load cell tension allows the work to be calculated within each time step. As the sampling rates varied between the video imaging and load cell, the load cell data was fit to an eighth-order polynomial, providing an accurate correlation of the load cell values to the same time-step as the video imaging. This ensured that the recording times for both the load cell and video were synchronized.

Instantaneous work was calculated within all seven shots by multiplying the recorded load cell value for each time step by the back face deflection during each time step. Once the summation through the recorded motion is completed the total work is calculated through the summation of the instantaneous work values collected within each time step.

As a comparison, the kinetic energy, based on the initial back face velocity, was determined. Using a final velocity of zero an approximation of the energy stored can be calculated. This energy value will only use the mass of the projectile and will not consider the inertia of the textile backing, providing a lower estimate of the energy imparted on the textile backing material. This value can serve as a grounding for the calculated work performed.

THIS PAGE INTENTIONALLY LEFT BLANK

IV. DATA

For the purpose of this thesis, multiple combinations of differing ceramic front face armor systems were paired with an 80-layer UHMWPE polymer backing and tested under rapid impact loading tests by two different projectiles, seen previously in Table 2. All targets were mounted and engaged at a breech pressure of 4000 psi with corresponding incident velocities, as described in Table 3.

Table 3. Shot Sequence

Shot #	Target Description (Ceramic Front Face)	Target Description (Polymer Backing)	Projectile	Projectile Stopped	Velocity (m/s)	Bullet Mass (g)	Sample Rate (FPS)	Pixel Size
1	SiC Tile	80-Layer UHMWPE	AK-47	Yes	634.99	7.835	206349.2115	256x128
2	3/8 Spheres AD995	80-Layer UHMWPE	AK-47	No	631.54	7.854	206349.2115	256x128
3	3/8 Spheres AD90	80-Layer UHMWPE	AK-47	No	627.42	8.017	206349.2115	256x128
4	3/8 Spheres AD90 (Al Encased)	80-Layer UHMWPE	AK-47	No	600.27	7.487	206349.2115	256x128
5	3/8 Spheres AD90 (P1000 Encased)	80-Layer UHMWPE	AK-47	No	622.68	7.843	206349.2115	256x128
6	3/8 Spheres AD90	80-Layer UHMWPE	M80	Yes	548.64	9.586	153664.3064	384x288
7	SiC Tile	80-Layer UHMWPE	M80	Yes	587.61	9.575	153664.3064	384x288

A. LOAD CELL DATA

Complete load cell datasets were obtained for all shots as a function of pounds of force. Units were converted to force in Newtons. However, upon inspection of the load cell data, it was found that the load cell for the Y axis displayed faulty data after its incident load cell force peak. This resulted in false returns after its initial upward spike. Thus, for Figures 36 to 42 only X axis values for load are displayed but remain representative of Y axis load values from the beginning of load cell recording until the time of incident peaks in each case. Force measurements were recorded over a range of 5000 data points with a 2 μs sampling period for a total indexed time of 0.01 s. For the scope of this experiment, only the first 1000 time steps will be considered as this initial impact measurement from 0 to

.002 s is the realm of interest. Figures 36 to 42 represent the load cell force measurements in Newtons over time in seconds for Shots 1-7, respectively.

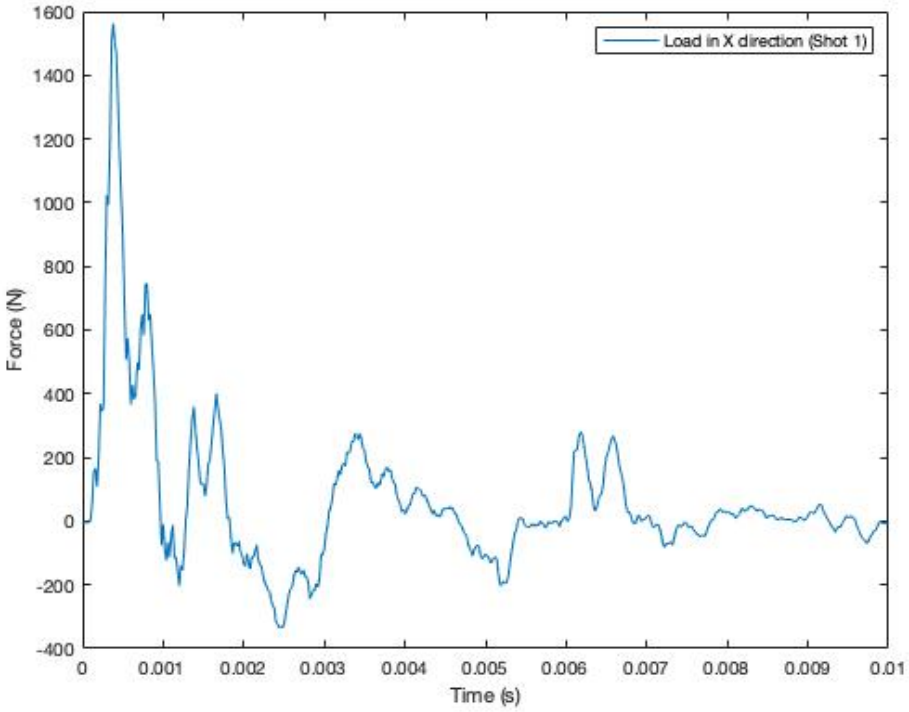

Figure 36. Load Cell Measurement: Shot 1 - SiC 7.2 x 7.2 cm tile 0.635 cm thickness with 80-Layer UHMWPE backing/ AK-47 Ball (7.62x39 mm) Projectile / 4000 psi

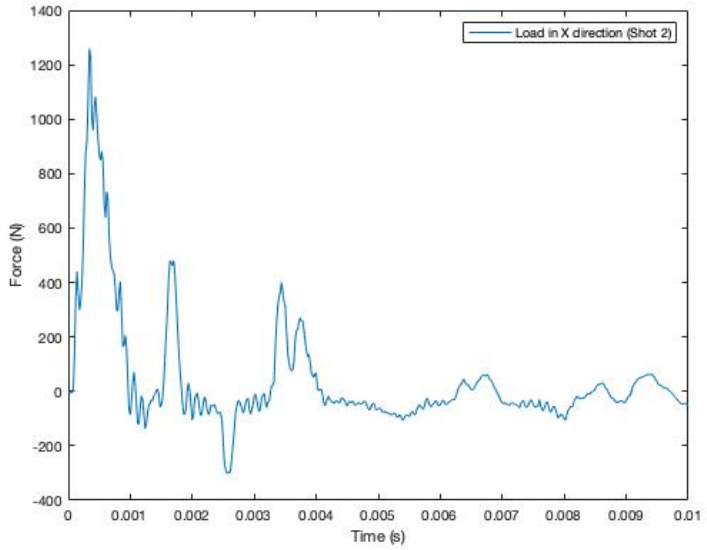

Figure 37. Load Cell Measurement: Shot 2 - Al_2O_3 AD995 7.62 x 7.62 cm 4 Row 0.953 cm thickness with 80-Layer UHMWPE backing/ AK-47 Ball (7.62x39 mm) Projectile / 4000 psi

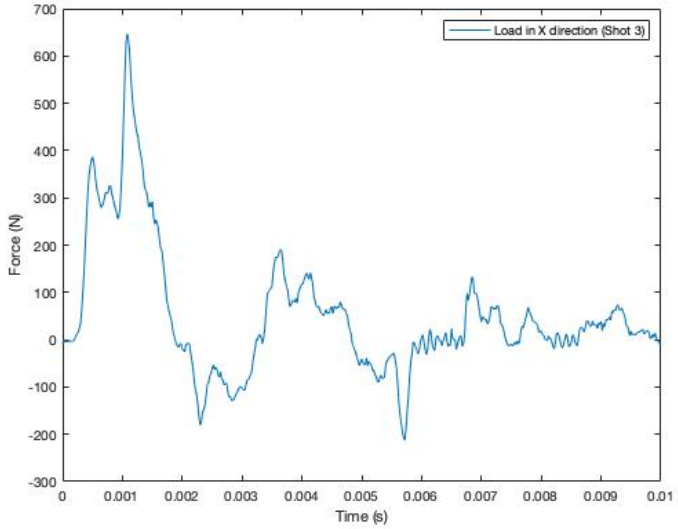

Figure 38. Load Cell Measurement: Shot 3 - Al_2O_3 AD90 7.62 x 7.62 cm 4 Row 0.953 cm thickness with 80-Layer UHMWPE backing/ AK-47 Ball (7.62x39 mm) Projectile / 4000 psi

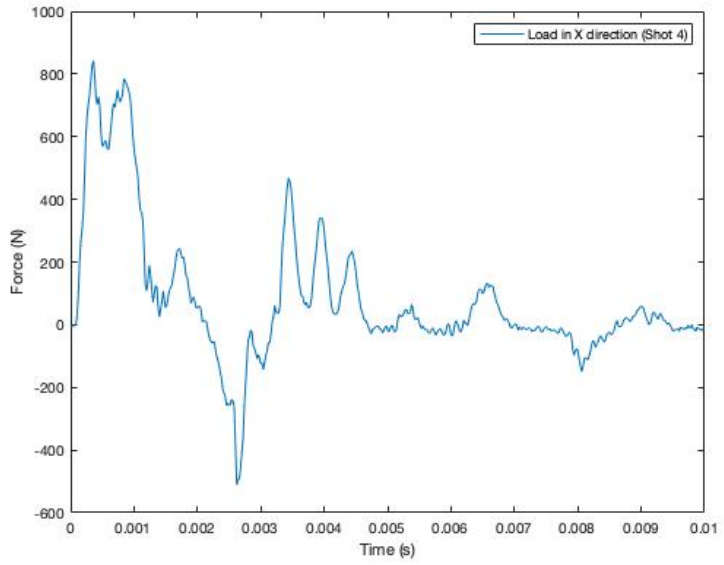

Figure 39. Load Cell Measurement: Shot 4 - Al Encapsulated Al_2O_3 AD90 0.953 cm thickness with 80-Layer UHMWPE backing/ AK-47 Ball (7.62x39 mm) Projectile / 4000 psi

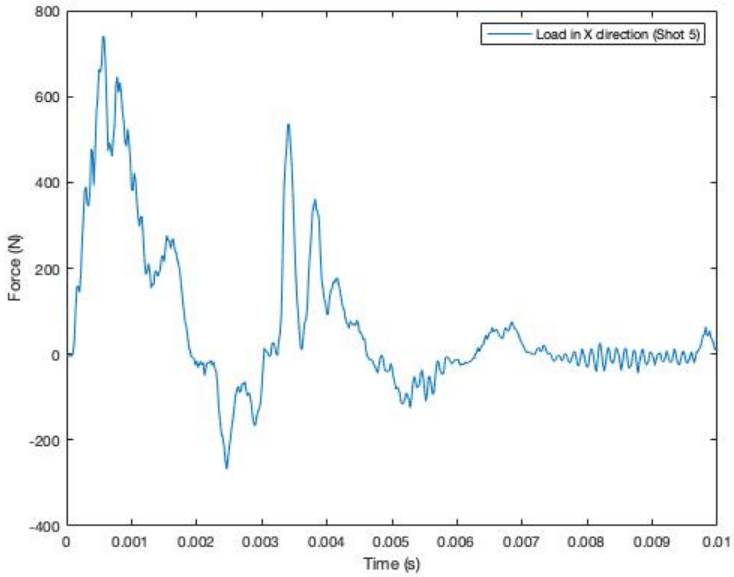

Figure 40. Load Cell Measurement: Shot 5 – P1000 Encapsulated Al_2O_3 AD90 0.953 cm thickness with 80-Layer UHMWPE backing/ AK-47 Ball (7.62x39 mm) Projectile / 4000 psi

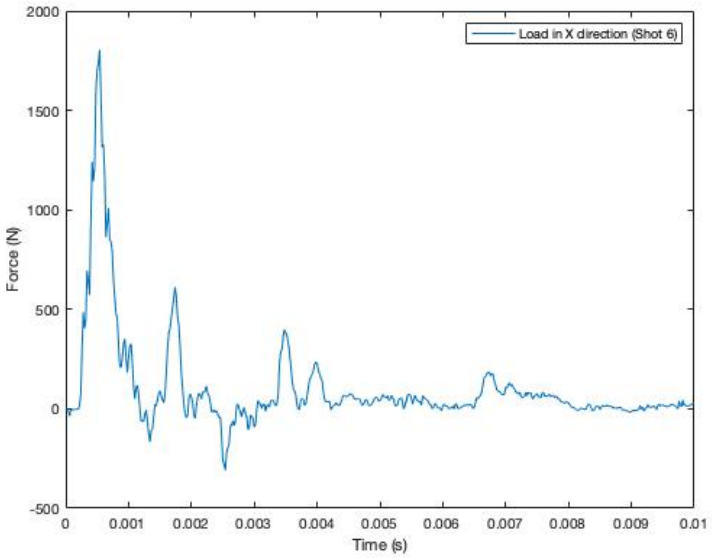

Figure 41. Load Cell Measurement: Shot 6 - Al_2O_3 AD90 7.62 x 7.62 cm 4 Row 0.953 cm thickness with 80-Layer UHMWPE backing/ M80 Ball (7.62x51 mm) Projectile / 4000 psi

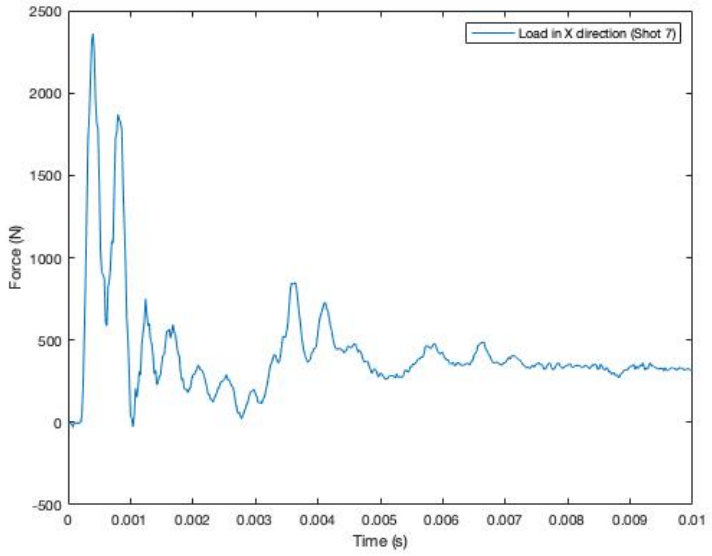

Figure 42. Load Cell Measurement: Shot 7 - SiC 7.2 x 7.2 cm tile 0.635 cm thickness with 80-Layer UHMWPE backing/ M80 Ball (7.62x51 mm) Projectile / 4000 psi

B. TEMA MEASUREMENTS

High-speed video was collected and analyzed via the TEMA 2D tracking program. Once video files were uploaded into the TEMA program, proper video camera settings were selected. These settings varied slightly after Shot 5 in an effort to increase clarity in the recorded image; these variations included reducing the sample rate from 206,349.2115 fps to 153,664.3064 fps and adjusting the pixel size from 256 x 128 to 384 x 288. Tables 4 to 14 depict the recorded advance in the transverse wave in millimeters in the X direction as well as the back face deformation in millimeters in the Z direction at the time indicated for each concurrent image for all shots performed. This time stamp for each image is a function of one over the sample rate, thus the sample rates of 206,349.2115 fps and 153,664.3064 yield deltas for time of 4.846 μs and 6.508 μs respectively. Theta values were calculated for each shot that had corresponding X and Z values in the same frame; this value can be used to further analyze the strain that the fiber system is experiencing. The wave propagation measurements, displayed in Tables 4 to 10 for Shot 1 to 7, are also plotted in Figures 43-56 presenting propagation distance vs. time in order to derive velocities that will be later discussed.

Table 4. TEMA Measurements: Shot 1 - SiC 7.2 x 7.2 cm tile 0.635 cm thickness with 80-Layer UHMWPE backing/ AK-47 Ball (7.62x39 mm) Projectile / 4000 psi

Time (s)	HorizPos (mm)	VertPos (mm)	VerticalVel (m/s)	Angle (deg)
1.454E-5	2.18562	3.18108	343.71206	49.59464
1.938E-5	4.37123	4.90226	321.43854	44.98014
2.423E-5	6.55685	6.51245	300.40348	40.20602
2.908E-5	8.74246	8.01774	280.57048	38.17069
3.392E-5	10.92808	9.42405	261.90315	35.75612
3.877E-5	13.11369	10.73711	244.36507	35.31832
4.362E-5	15.29931	11.9625	227.91987	33.81358
4.846E-5	17.48492	13.10558	212.53112	33.60657
5.331E-5	19.67054	14.17156	198.16245	33.23363
5.815E-5	21.85615	15.16549	184.77745	31.98888
6.3E-5	24.04177	16.09222	172.33972	31.517
6.785E-5	26.22738	16.95641	160.81287	32.2299
7.269E-5	28.413	17.76259	150.1605	31.11345
7.754E-5	30.59861	18.51506	140.3462	30.52461
8.238E-5	32.78423	19.21799	131.33358	29.5226
8.723E-5	34.96985	19.87534	123.08625	28.62258
9.208E-5	37.15546	20.49091	115.5678	27.82754
9.692E-5	39.34108	21.06833	108.74184	27.16184
1.0177E-4	41.52669	21.61103	102.57196	26.35999

Time (s)	HorizPos (mm)	VertPos (mm)	VerticalVel (m/s)	Angle (deg)
1.0662E-4	43.71231	22.12229	97.02178	25.69797
1.1146E-4	45.89792	22.60519	92.05488	24.99285
1.1631E-4	48.08354	23.06265	87.63488	24.91553
1.2115E-4	50.26915	23.49741	83.72538	24.36223
1.26E-4	52.45477	23.91204	80.28997	23.97005
1.3085E-4	54.64038	24.30891	77.29227	23.46309
1.3569E-4	56.826	24.69023	74.69586	22.88491
1.4054E-4	59.01161	25.05805	72.46436	22.18906
1.4538E-4	61.19723	25.41421	70.56136	21.88128
1.5023E-4	63.38284	25.76039	68.95047	21.33357
1.5508E-4	65.56846	26.09811	67.59529	20.87089
1.5992E-4	67.75408	26.42868	66.45942	20.45337
1.6477E-4	69.93969	26.75326	65.50647	20.35415

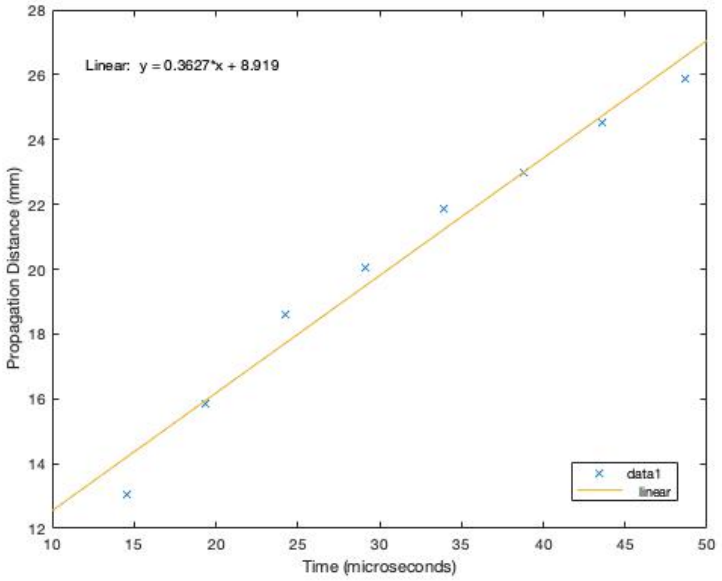

Figure 43. Transverse Wave Data: Shot 1 - SiC 7.2 x 7.2 cm tile 0.635 cm thickness with 80-Layer UHMWPE backing/ AK-47 Ball (7.62x39 mm) Projectile / 4000 psi

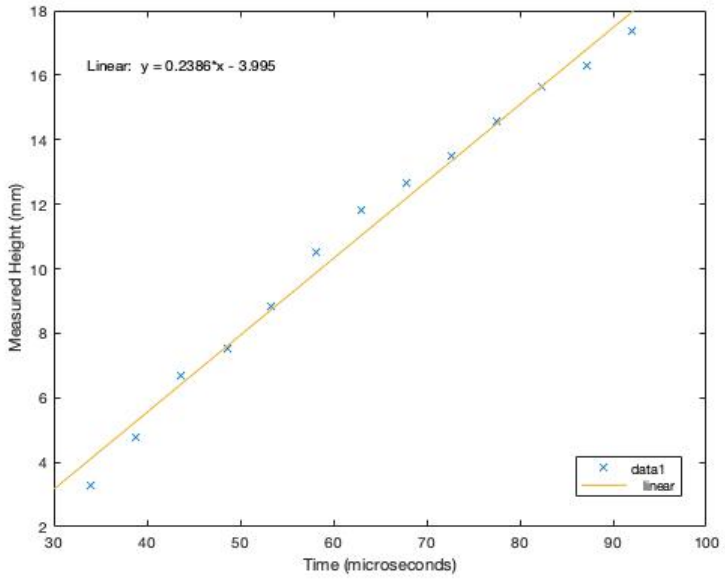

Figure 44. Back Face Deformation Wave Data: Shot 1 - SiC 7.2 x 7.2 cm tile 0.635 cm thickness with 80-Layer UHMWPE backing/ AK-47 Ball (7.62x39 mm) Projectile / 4000 psi

Table 5. TEMA Measurements: Shot 2 - Al_2O_3 AD995 7.62 x 7.62 cm 4 Row 0.953 cm thickness with 80-Layer UHMWPE backing/ AK-47 Ball (7.62x39 mm) Projectile / 4000 psi

Time (s)	HorizPos (mm)	VertPos (mm)	VerticalVel (m/s)	Angle (deg)
1.454E-5	2.9707	1.00668	215.07323	18.92984
1.938E-5	5.94139	1.95216	250.93215	17.89827
2.423E-5	8.91209	3.09124	279.17526	18.80474
2.908E-5	11.88278	4.38427	300.94069	18.64898
3.392E-5	14.85348	5.7971	317.36658	20.92537
3.877E-5	17.82417	7.30109	329.59103	23.28908
4.362E-5	20.79487	8.87312	338.75219	21.78049
4.846E-5	23.76556	10.49559	345.98818	23.03966
5.331E-5	26.73626	12.15641	352.43712	23.7716
5.815E-5	29.70695	13.84901	359.23713	23.87032
6.3E-5	32.67765	15.57234	367.52636	24.63537
6.785E-5	35.64834	17.33085		25.47916
7.269E-5	38.61904	19.13452		25.24585

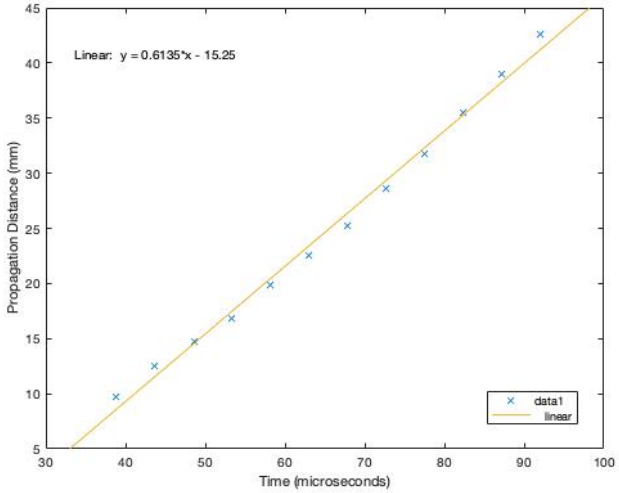

Figure 45. Transverse Wave Data: Shot 2 - Al_2O_3 AD995 7.62 x 7.62 cm 4 Row 0.953 cm thickness with 80-Layer UHMWPE backing/ AK-47 Ball (7.62x39 mm) Projectile / 4000 psi

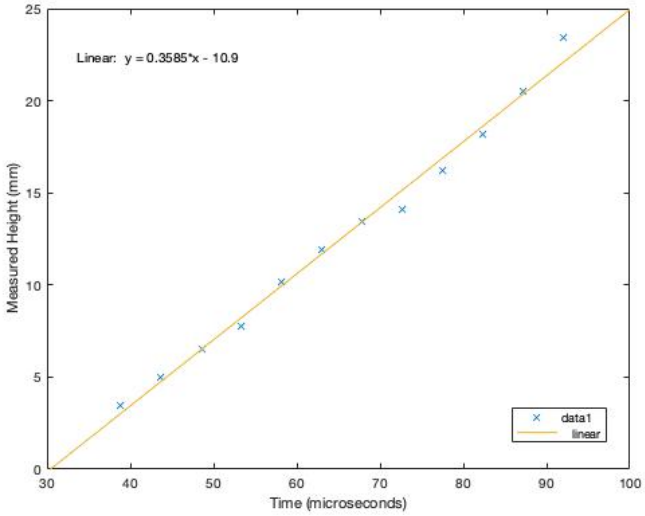

Figure 46. Back Face Deformation Wave Data: Shot 2 - Al_2O_3 AD995 7.62 x 7.62 cm 4 Row 0.953 cm thickness with 80-Layer UHMWPE backing/ AK-47 Ball (7.62x39 mm) Projectile / 4000 psi

Table 6. TEMA Measurements: Shot 3 - Al_2O_3 AD90 7.62 x 7.62 cm 4 Row 0.953 cm thickness with 80-Layer UHMWPE backing/ AK-47 Ball (7.62x39 mm) Projectile / 4000 psi

Time (s)	HorizPos (mm)	VertPos (mm)	VerticalVel (m/s)	Angle (deg)
1.454E-5	2.29708	4.15747	156.1648	50.22899
1.938E-5	4.59415	4.7896	205.16841	40.93078
2.423E-5	6.89123	5.67107	249.32837	36.89301
2.908E-5	9.18831	6.77816	288.73887	33.72598
3.392E-5	11.48538	8.08763	323.49411	33.07422
3.877E-5	13.78246	9.57671	353.68829	32.85978
4.362E-5	16.07954	11.22304	379.41559	32.50607
4.846E-5	18.37661	13.00476	400.77023	33.2218
5.331E-5	20.67369	14.90045		33.51594
5.815E-5	22.97077	16.88915		

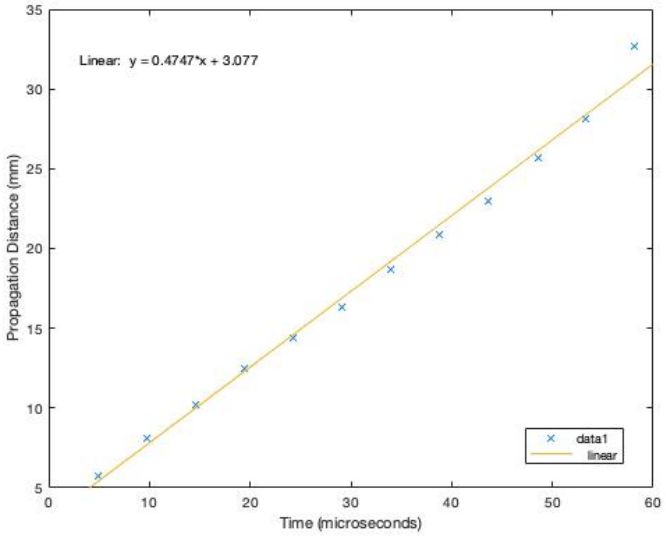

Figure 47. Transverse Wave Data: Shot 3 - Al_2O_3 AD90 7.62 x 7.62 cm 4 Row 0.953 cm thickness with 80-Layer UHMWPE backing/ AK-47 Ball (7.62x39 mm) Projectile / 4000 psi

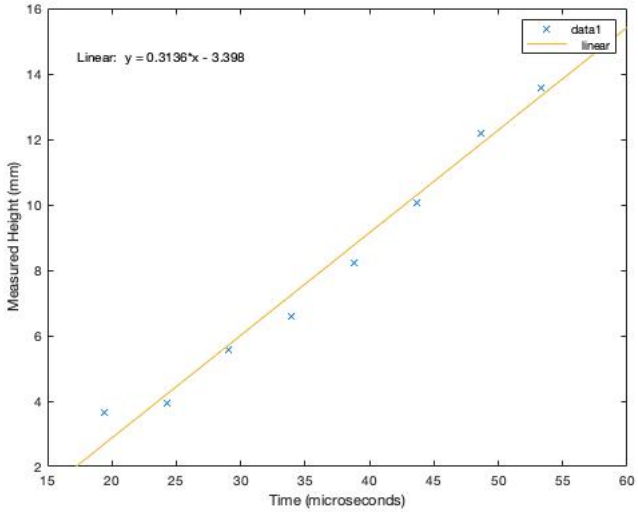

Figure 48. Back Face Deformation Wave Data: Shot 3 - Al_2O_3 AD90 7.62 x 7.62 cm 4 Row 0.953 cm thickness with 80-Layer UHMWPE backing/ AK-47 Ball (7.62x39 mm) Projectile / 4000 psi

Table 7. TEMA Measurements: Shot 4 - Al Encapsulated Al_2O_3 AD90 0.953 cm thickness with 80-Layer UHMWPE backing/ AK-47 Ball (7.62x39 mm) Projectile / 4000 psi

Time (s)	HorizPos (mm)	VertPos (mm)	VerticalVel (m/s)	Angle (deg)
1.454E-5	2.61208	1.87658	213.32417	31.84976
1.938E-5	5.22416	2.7076	276.7852	28.67559
2.423E-5	7.83624	3.94418	304.65248	25.33566
2.908E-5	10.44832	5.39029	306.63701	25.55106
3.392E-5	13.0604	6.89697	292.4498	26.79279
3.877E-5	15.67248	8.36231	271.80184	26.8233
4.362E-5	18.28456	9.73149	254.40414	27.17754
4.846E-5	20.89664	10.9967	249.9677	27.0232
5.331E-5	23.50872	12.19725	268.20351	26.17266
5.815E-5	26.1208	13.41947		25.98751
6.3E-5	28.73287	14.79676		26.34388

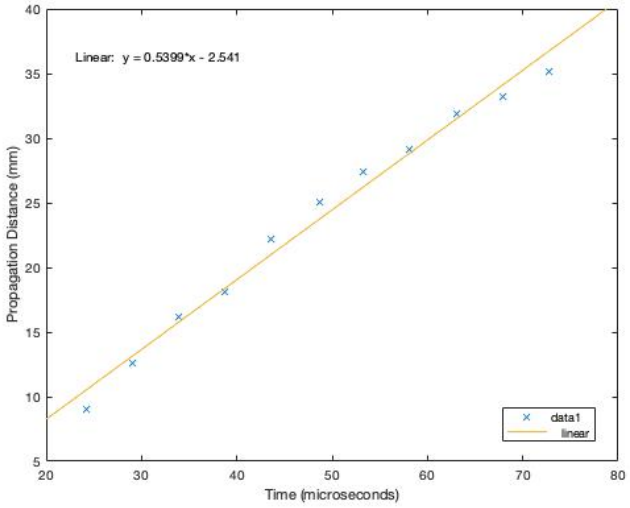

Figure 49. Transverse Wave Data: Shot 4 - Al Encapsulated Al_2O_3 AD90 0.953 cm thickness with 80-Layer UHMWPE backing/ AK-47 Ball (7.62x39 mm) Projectile / 4000 psi

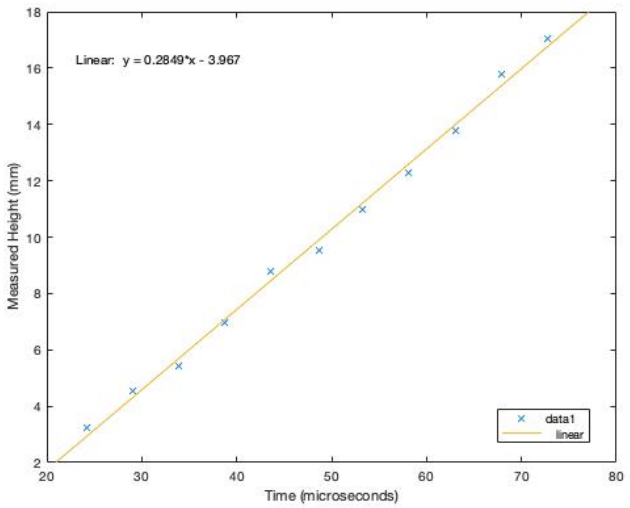

Figure 50. Back Face Deformation Wave Data: Shot 4 - Al Encapsulated Al_2O_3 AD90 0.953 cm thickness with 80-Layer UHMWPE backing/ AK-47 Ball (7.62x39 mm) Projectile / 4000 psi

Table 8. TEMA Measurements: Shot 5 – P1000 Encapsulated Al_2O_3 AD90 0.953 cm thickness with 80-Layer UHMWPE backing/ AK-47 Ball (7.62x39 mm) Projectile / 4000 psi

Time (s)	HorizPos (mm)	VertPos (mm)	VerticalVel (m/s)	Angle (deg)
1.454E-5	5.81054	1.76569	69.76636	16.04013
1.938E-5	11.62109	1.80278	173.35782	9.17948
2.423E-5	17.43163	2.44189	239.44284	8.95364
2.908E-5	23.24218	3.48302	275.54098	7.17145
3.392E-5	29.05272	4.76264	289.17181	9.18622
3.877E-5	34.86327	6.15365	287.85489	10.76893
4.362E-5	40.67381	7.56539	279.1098	10.03854
4.846E-5	46.48435	8.94363	270.4561	10.97122
5.331E-5	52.2949	10.27061		11.02488
5.815E-5	58.10544	11.56498		11.11651

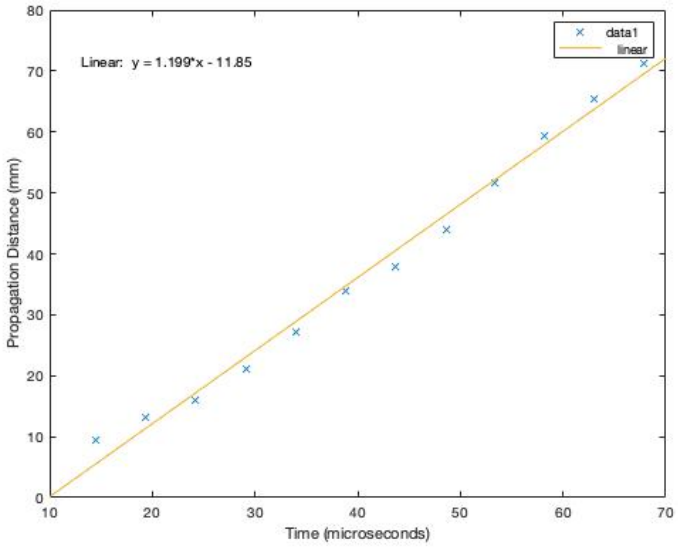

Figure 51. Transverse Wave Data: Shot 5 – P1000 Encapsulated Al_2O_3 AD90 0.953 cm thickness with 80-Layer UHMWPE backing/ AK-47 Ball (7.62x39 mm) Projectile / 4000 psi

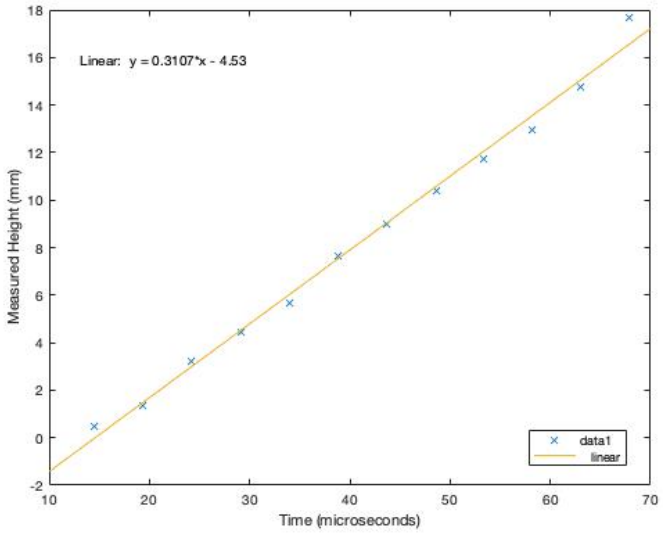

Figure 52. Back Face Deformation Wave Data: Shot 5 – P1000 Encapsulated Al_2O_3 AD90 0.953 cm thickness with 80-Layer UHMWPE backing/ AK-47 Ball (7.62x39 mm) Projectile / 4000 psi

Table 9. TEMA Measurements: Shot 6 - Al_2O_3 AD90 7.62 x 7.62 cm 4 Row 0.953 cm thickness with 80-Layer UHMWPE backing/ M80 Ball (7.62x51 mm) Projectile / 4000 psi

Time (s)	HorizPos (mm)	VertPos (mm)	VerticalVel (m/s)	Angle (deg)
1.454E-5	2.31674	3.97209	198.20057	50.35193
1.938E-5	4.63349	5.22839	207.27689	42.49892
2.423E-5	6.95023	6.55175	213.97124	38.04358
2.908E-5	9.26697	7.92618	218.43049	37.01382
3.392E-5	11.58372	9.33667	220.80153	36.00523
3.877E-5	13.90046	10.76915	221.23122	34.86958
4.362E-5	16.2172	12.2105	219.86645	34.64202
4.846E-5	18.53394	13.64856	216.85408	34.67906
5.331E-5	20.85069	15.07215	212.341	33.77739
5.815E-5	23.16743	16.47101	206.47407	33.05734
6.3E-5	25.48417	17.83585	199.40017	32.79787
6.785E-5	27.80092	19.15835	191.26619	32.57933
7.269E-5	30.11766	20.43113	182.21898	32.2016
7.754E-5	32.4344	21.64776	172.40544	31.71425
8.238E-5	34.75115	22.80278	161.97242	31.19735
8.723E-5	37.06789	23.89169	151.06681	30.90089
9.208E-5	39.38463	24.91092	139.83549	30.5188
9.692E-5	41.70137	25.85788	128.42533	30.07057
1.0177E-4	44.01812	26.73094	116.98319	29.87106

Time (s)	HorizPos (mm)	VertPos (mm)	VerticalVel (m/s)	Angle (deg)
1.0662E-4	46.33486	27.52939	105.65597	29.6558
1.1146E-4	48.6516	28.25352	94.59053	28.84853
1.1631E-4	50.96835	28.90455	83.93375	28.24286
1.2115E-4	53.28509	29.48466	73.8325	27.63852
1.26E-4	55.60183	29.99698	64.43367	27.10529
1.3085E-4	57.91858	30.44562	55.88411	26.71339
1.3569E-4	60.23532	30.83561	48.33072	26.06427
1.4054E-4	62.55206	31.17297	41.92036	25.46644
1.4538E-4	64.8688	31.46465	36.79991	25.04531
1.5023E-4	67.18555	31.71858	33.11624	24.55755
1.5508E-4	69.50229	31.94362		23.93146
1.5992E-4	71.81903	32.1496		23.37015

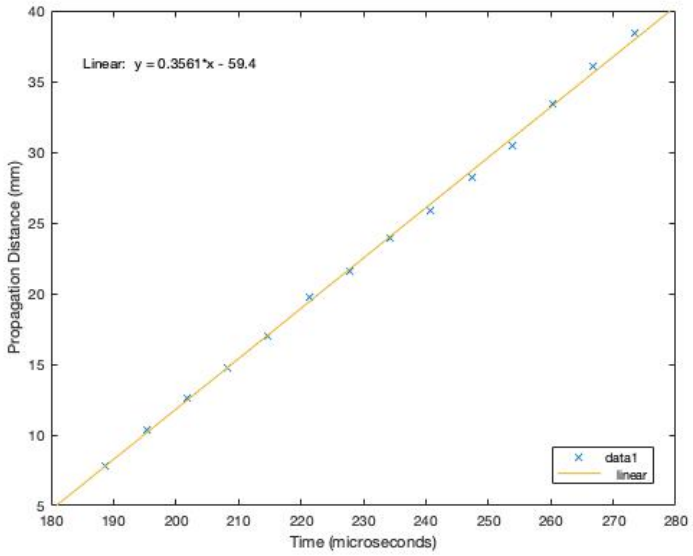

Figure 53. Transverse Wave Data: Shot 6 - Al_2O_3 AD90 7.62 x 7.62 cm 4 Row 0.953 cm thickness with 80-Layer UHMWPE backing/ M80 Ball (7.62x51 mm) Projectile / 4000 psi

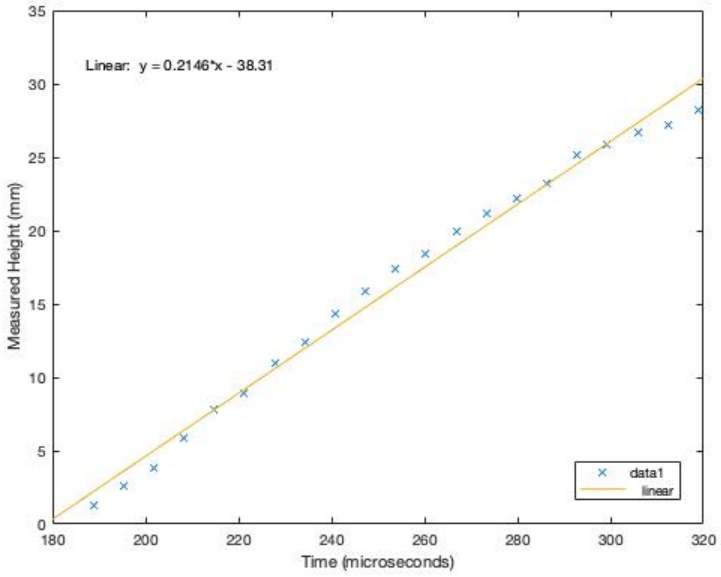

Figure 54. Back Face Deformation Wave Data: Shot 6 - Al_2O_3 AD90 7.62 x 7.62 cm 4 Row 0.953 cm thickness with 80-Layer UHMWPE backing/ M80 Ball (7.62x51 mm) Projectile / 4000 psi

Table 10. TEMA Measurements: Shot 7 - SiC 7.2 x 7.2 cm tile 0.635 cm thickness with 80-Layer UHMWPE backing/ M80 Ball (7.62x51 mm) Projectile / 4000 psi

Time (s)	HorizPos (mm)	VertPos (mm)	VerticalVel (m/s)	Angle (deg)
1.454E-5	2.92196	2.00759	192.82769	38.41168
1.938E-5	5.84392	3.26962	190.34256	27.95149
2.423E-5	8.76588	4.51732	187.3042	23.36319
2.908E-5	11.68784	5.747	183.74274	24.00957
3.392E-5	14.6098	6.95516	179.68829	24.25908
3.877E-5	17.53176	8.13849	175.17098	24.09243
4.362E-5	20.45372	9.29388	170.22091	23.85387
4.846E-5	23.37568	10.41841	164.86822	23.24991
5.331E-5	26.29764	11.50937	159.14303	22.33084
5.815E-5	29.2196	12.56424	153.07544	22.64916
6.3E-5	32.14156	13.58069	146.69559	23.03274
6.785E-5	35.06352	14.55658	140.03359	22.67797
7.269E-5	37.98547	15.48999	133.11956	21.80928
7.754E-5	40.90743	16.37917	125.98362	21.56036
8.238E-5	43.82939	17.22259	118.65589	21.18875
8.723E-5	46.75135	18.0189	111.16649	20.47615
9.208E-5	49.67331	18.76695	103.54554	20.37726
9.692E-5	52.59527	19.46578	95.82316	19.8611
1.0177E-4	55.51723	20.11464	88.02946	19.287

Time (s)	HorizPos (mm)	VertPos (mm)	VerticalVel (m/s)	Angle (deg)
1.0662E-4	58.43919	20.71296	80.19458	18.79298
1.1146E-4	61.36115	21.26038	72.34862	18.59402
1.1631E-4	64.28311	21.75672	64.52172	17.96288
1.2115E-4	67.20507	22.20202	56.74398	17.64825
1.26E-4	70.12703	22.5965	49.04552	17.5077
1.3085E-4	73.04899	22.94057	41.45648	17.11341
1.3569E-4	75.97095	23.23485	34.00695	17.08837
1.4054E-4	78.89291	23.48014	26.72708	16.67554
1.4538E-4	81.81487	23.67746	19.64697	16.34589
1.5023E-4	84.73683	23.82801	12.79675	15.82595
1.5508E-4	87.65879	23.93318		14.66823
1.5992E-4	90.58075	23.99456		14.48591

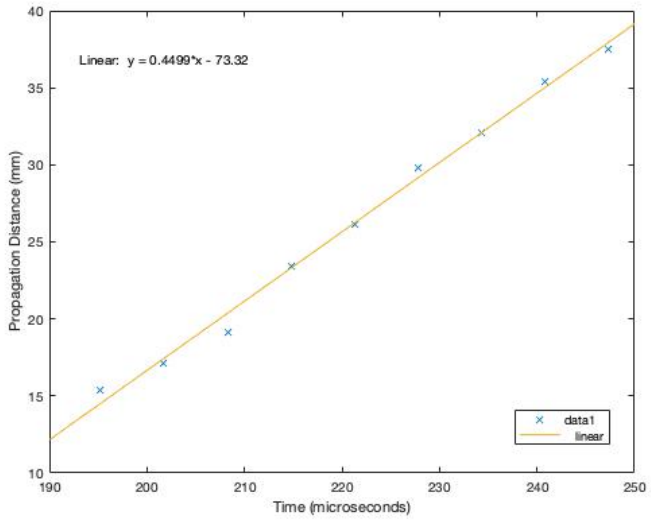

Figure 55. Transverse Wave Data: Shot 7 - SiC 7.2 x 7.2 cm tile 0.635 cm thickness with 80-Layer UHMWPE backing/ M80 Ball (7.62x51 mm) Projectile / 4000 psi

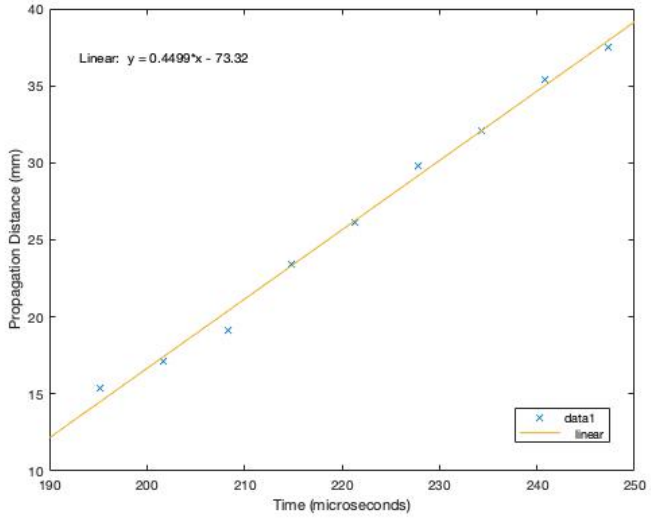

Figure 56. Back Face Deformation Wave Data: Shot 7 - SiC 7.2 x 7.2 cm tile 0.635 cm thickness with 80-Layer UHMWPE backing/ M80 Ball (7.62x51 mm) Projectile / 4000 psi

C. PENETRATION MEASUREMENTS

To properly assess the residual damage to the body armor system, an analysis of penetration depth was conducted for all shots. This analysis examined the penetration depth as a percentage weight of the center 7.62 x 7.62 cm target square by peeling back layers until no more layers are physically observed to contain penetration from the projectile. Care was taken to ensure even removal of layers. Weights were taken before and after removal of the penetrated layers to generate this percentage. Shots 2-5 were complete penetration of the UHMWPE backing and are thus assigned a value of 100% for penetration. Values for all other Shots are provided in Table 11 below including: mass pre-removal of severed layers, mass post-removal of severed layers, the percent penetration, and the approximated number of layers this equates to. The percent penetration of the UHMWPE backing calculated is also plotted in Figure 57 for the respective ceramic front faces.

Table 11. Penetration Test Results

Shot #	Mass Pre Removal (g)	Mass Post Removal (g)	% Penetration	Approx. # Layers
1	30.142	15.106	49.88	40
2	-	-	100	-
3	-	-	100	-
4	-	-	100	-
5	-	-	100	-
6	27.844	23.802	14.52	12
7	28.196	19.051	32.43	26

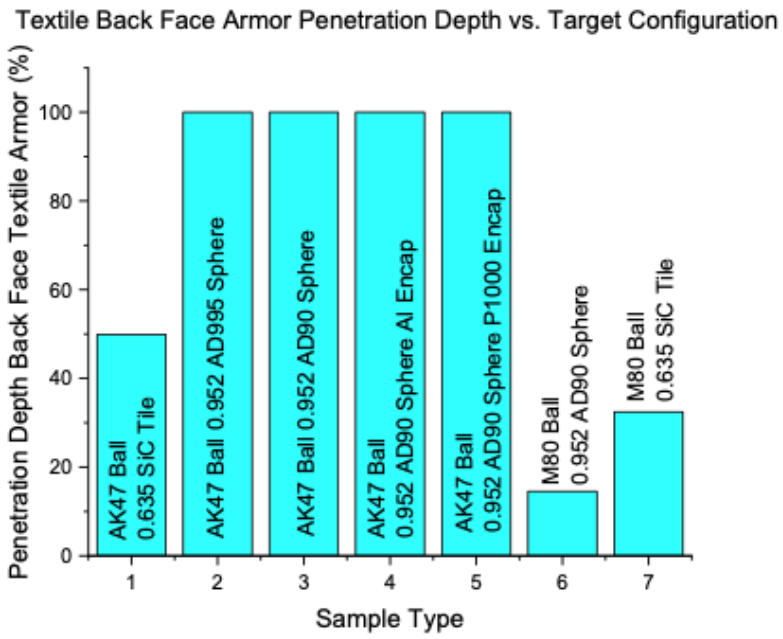

Figure 57. Back Face Penetration Percentage Shot Comparison

THIS PAGE INTENTIONALLY LEFT BLANK

V. DATA ANALYSIS

Much analysis for the purpose of this thesis was derived from Smith's study of wave propagation in a single fiber due to rapid impact loading at a transverse angle to the plane of interest [16]. Analyzing the deformations in the X and Z directions relative to the plane of interest as gathered in Chapter IV allowed for comparison to the Smith paper [16]. Some assumptions will be addressed appropriately as they relate to the relevant information when calculating strain and tension from these wave propagation velocities. Furthermore, this tension will be compared to that experienced by the load cell upon impact to aid in understanding of the dependence of the backing system with the front face component.

A. WAVE VELOCITY ANALYSIS

As discussed previously, the transverse wave in the plane of the UHMWPE textile backing attenuates outwards in both the X and Y directions along the orientation of the fibers forming the square base of the tent formation at a rate of U recorded in mm/μs. Again, due to issues with the load cell in the Y axis, the propagation distance and concurrently the velocity (U) will only be described in terms of the X axis. Similarly, the height of the tent was recorded along the Z axis perpendicular to the target at a rate of V in mm/μs. Smith's paper states that in order for his equations presented to be used both U and V must be constant [16]. Thus, U and V were gathered analytically by plotting both propagation distances in the X and Z axis as functions of time and assign it a linear fit. These linear fits were observed in Figures 43-56; however, it is important to note that several plotted distances display some non-linear behavior. For the purpose of utilizing Smith's equations for comparison the linear fit will suffice, but a more in-depth study of how the effect of multiple fibers in height, width, and orientation could yield a more accurate result. From these linear fits, the U and V velocities were recorded by the slope of the trendline, and the results are recorded in Table 12 in m/s.

Table 12. Linear Fit Wave Velocities

Shot #	U (m/s)	V(m/s)
1	362.7	238.6
2	613.5	358.5
3	474.7	313.6
4	539.9	284.9
5	1199.0	310.7
6	356.1	214.6
7	449.9	193.1

From Table 12, though no discernable difference occurs in U for Shots 2-5 that experienced full penetration versus the rest of the shots, there is a trend that can be observed for V. This is displayed in Figure 58 by comparing V velocities for the different sample and round combinations. Repeated combinations are averaged for representation and clarity. For Shots 2-5 that experienced full penetration, there was a much higher back face deformation velocity (V > 250 m/s) relative to the other shots. This is indicative of larger kinetic energy values for the 7.62x39 mm AK-47 projectile then that of the 7.62x51 mm M80. In fact, Shot 1 against the SiC Tile by the AK-47 Ball 7.62x39 mm experienced a relatively high kinetic energy compared to the M80 projectiles even though it was completely stopped. This combination did produce a large amount of penetration damage as will be discussed later. Comparisons in the U velocities were irrelevant as the variance occurs for both full penetration as well as the stopped projectiles.

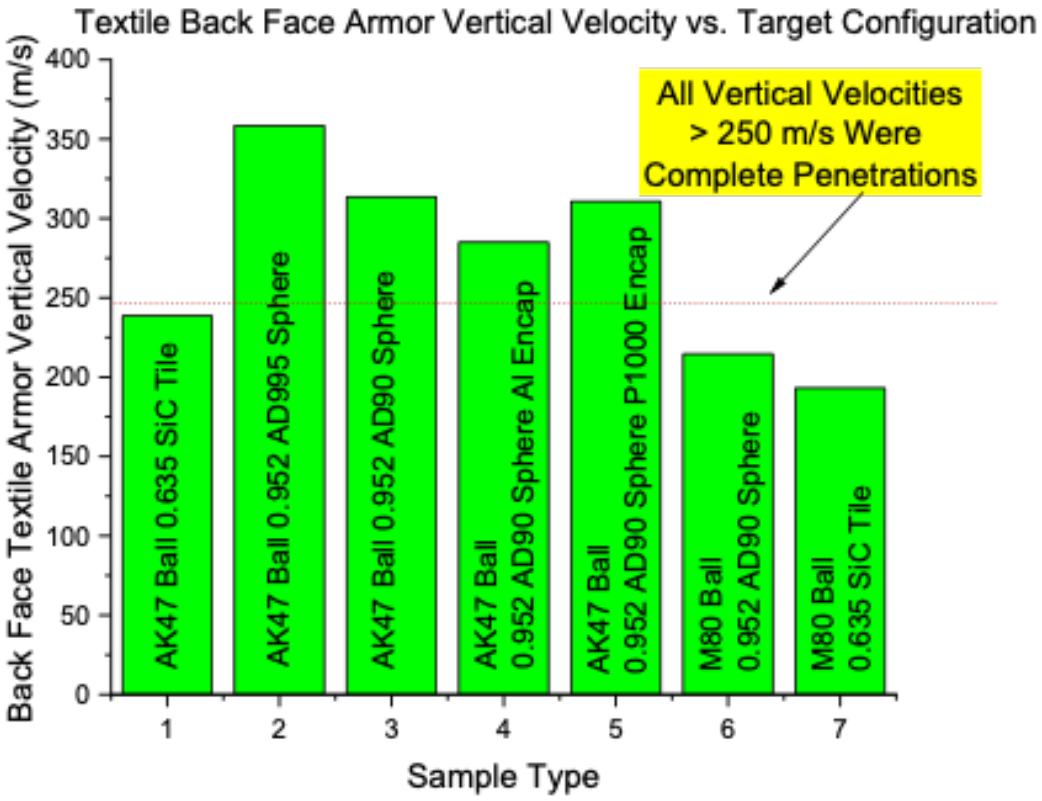

Figure 58. Back Face Velocity Shot Comparison

Though a linear fit was required to utilize the desired equations for comparison, it was evident in the data collected, from back face deflections, that some of the datasets were not best represented by linear fits and appear to demonstrate non-linear behavior. This was most evident for the V velocities for cases where the projectile was not stopped. Thus, to better understand what the V velocities are doing throughout the engagements, ΔX and ΔV were calculated from frame-to-frame for each Shot and compared as seen in Figure 67 and 68. Initial predictions were confirmed for the X direction for targets that stopped the projectile where ΔX would initially remain relatively constant but begin to taper off as seen in Figures 59 and 60.

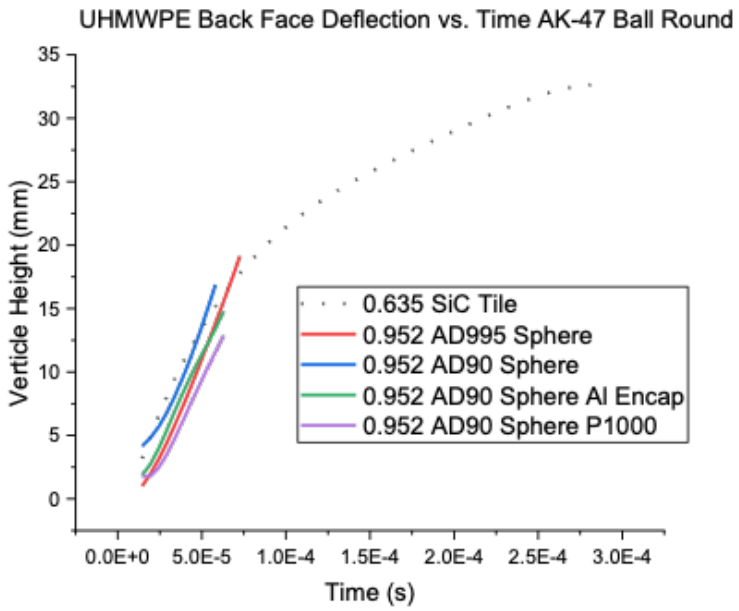

Figure 59. ΔX vs. Indexed Time: 7.62 x 39 mm (AK-47 Ball) Comparison.

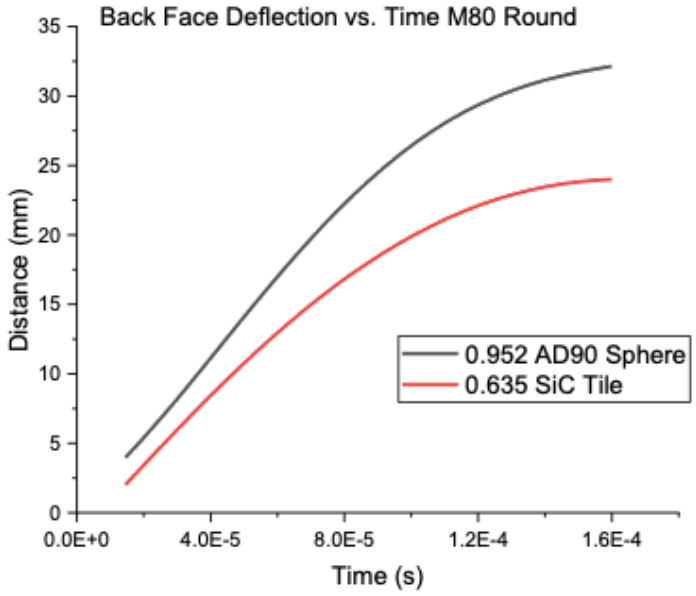

Figure 60. ΔX vs. Indexed Time: 7.62 x 51 mm (M80 Ball) Comparison.

Within Figure 59, for the four shots where complete penetration occurred, it is clear that the duration of the penetration was fairly consistent where a time period of just over 50 μs was required. From Figure 62 it becomes clear that, for all complete penetrations, the back face velocity continued to increase as opposed to targets that enabled partial penetration where a continuous decrease in back face velocity is observed. For the three shots that stopped the projectiles, we see downward slopes that constitute a reduction in velocity and kinetic energy over time, seen in Figures 61 and 63. For both instances involving the SiC tile, this reduction begins to occur immediately upon measured values. However, for the 0.952 cm AD90 ceramic spheres engaged with the M80 projectile, the back face velocity displayed a slight upward trend before its reduction that could be attributed to the difference in front face structure where no interlocking between the spheres occurs enabling additional forward momentum that was not observed for the ceramic tile targets during the projectile interaction with the front face system. In addition, the back face deflection for the AD90 spheres target had an additional ~1 cm deflection over the SiC tile supporting a higher kinetic energy imparted into the textile backing.

From this data it was also observed that encasement material provided minimal performance in penetration resistance. A final note regarding the back face deflection is the M80 appeared to be a lower threat even thought it had a higher threat. The core of the M80 is much softer than the AK-47 enabling additional front face surface deformation and reduced pressure on the textile backing material.

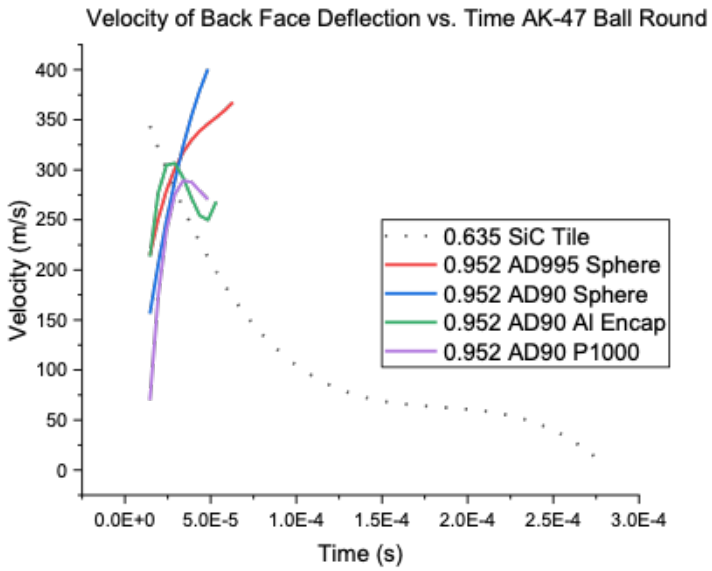

Figure 61. ΔV vs. Indexed Time: 7.62 x 39 mm (AK-47 Ball) Comparison.

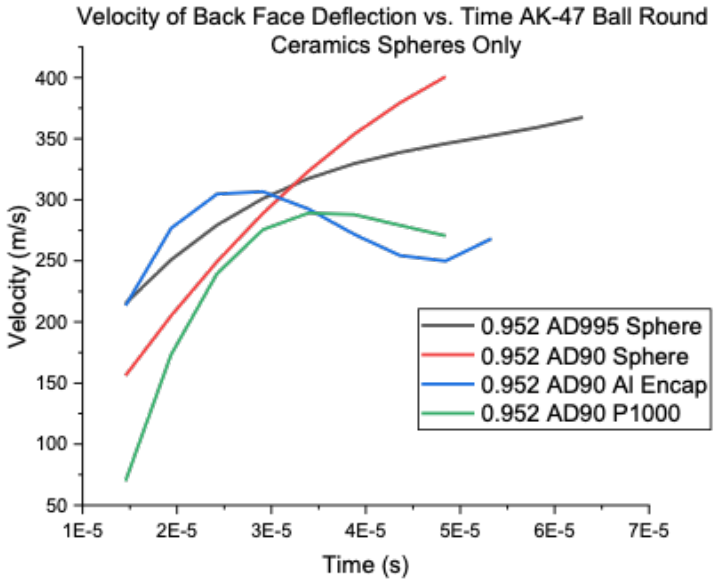

Figure 62. ΔV vs. Indexed Time: 7.62 x 39 mm (AK-47 Ball) Comparison (100% Penetrations).

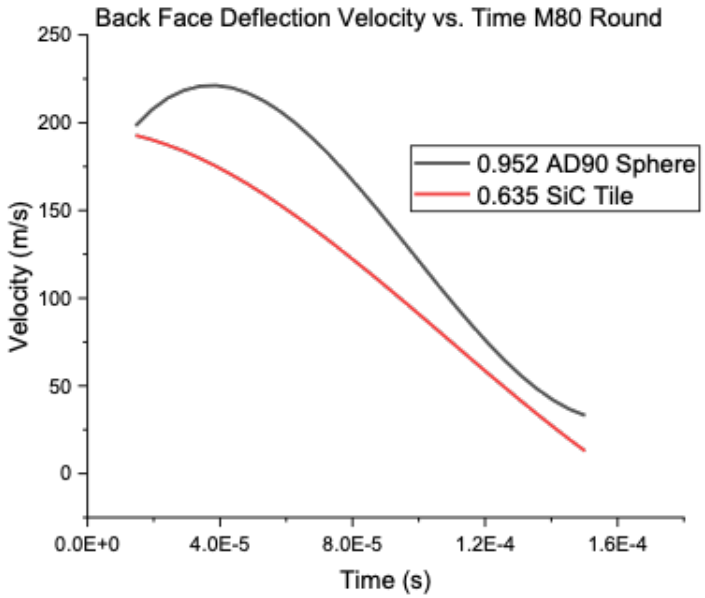

Figure 63. ΔV vs. Indexed Time: 7.62 x 51 mm (M80 Ball) Comparison.

B. LOAD CELL DATA ANALYSIS

Load cell data, presented earlier in Figures 36-42, was compiled according to the projectile type and displayed below in Figures 64 and 65 utilizing the first 1000 of the 5000 time steps for a better comparison. The data displayed in Figure 64 represents shots 1-5 with the 7.62x39 mm AK-47 projectile while Figure 65 represents Shots 6 and 7 with the 7.62x51 mm M80 projectile vs. their respective ceramic/polymer armor combinations.

From these datasets, only Shots 1, 6, and 7 stopped their projectiles and in turn incur the largest load cell force spikes at 1562 N, 1805 N, and 2360 N respectively. Shots 2-5 are observed to have a lower load on them as the body armor sample is applying less work on the incident projectile thus returning lower values for registered load via the load cells. Essentially, the projectile is cutting through the sample such that the load cells cannot register as much force on the sample. For the M80 projectiles displayed in Figure 65, it was observed that SiC tile experience a 555 N load difference over that of the AD90 ceramic sphere lattice. The M80 round severed approximately 26 layers of the UHMWPE backing after penetrating the SiC tile while the penetration after the AD90 spheres was approximately 12 layers. This difference in load suggests that SiC tile performed better in

both reducing the incident kinetic energy but may not have blunted the front face of the projectile reducing the pressure on the textile backing material to the same degree as the AD90 sphere. AD90 spheres which would also relate to less layers of penetration into the UHMWPE backing; however, this was not the case. This was an interesting result as though it failed to stop the AK-47 projectile it not only stopped the M80 round, but it outperformed the SiC Tile. Thus, according to this comparison, it is better suited for the NIJ Level III certification barring that its multi-hit capability remains intact as expected.

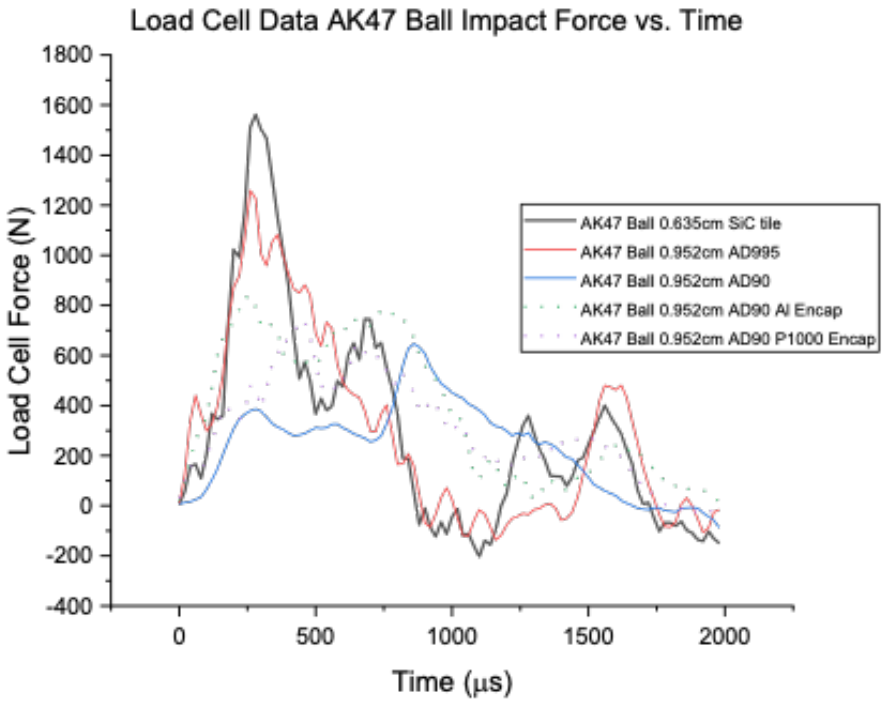

Figure 64. Compiled Load Cell Data: 7.62x39 mm Comparison.

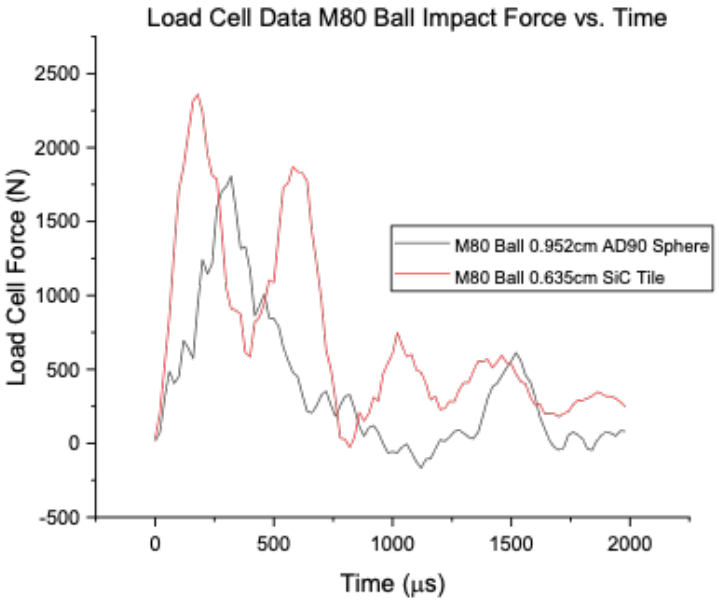

Figure 65. Compiled Load Cell Data: 7.62x51 mm Comparison.

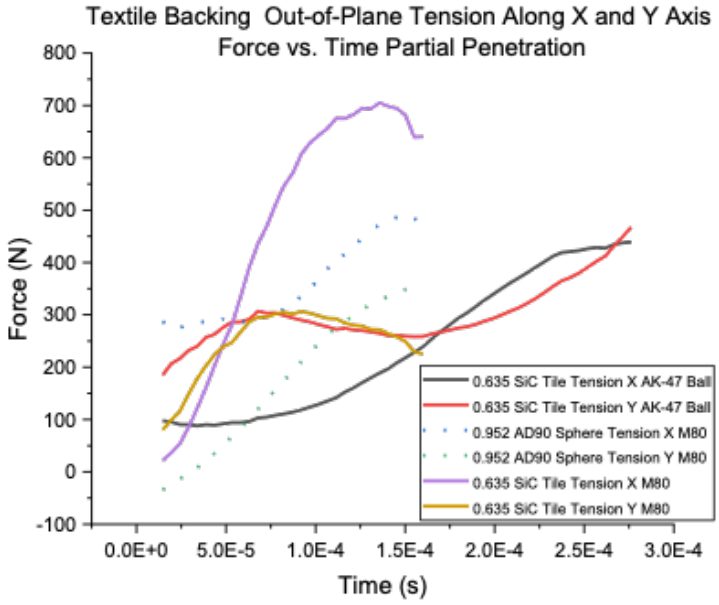

Figure 66. Tensile Force (T_p) vs. Indexed Time: Stopped Projectiles.

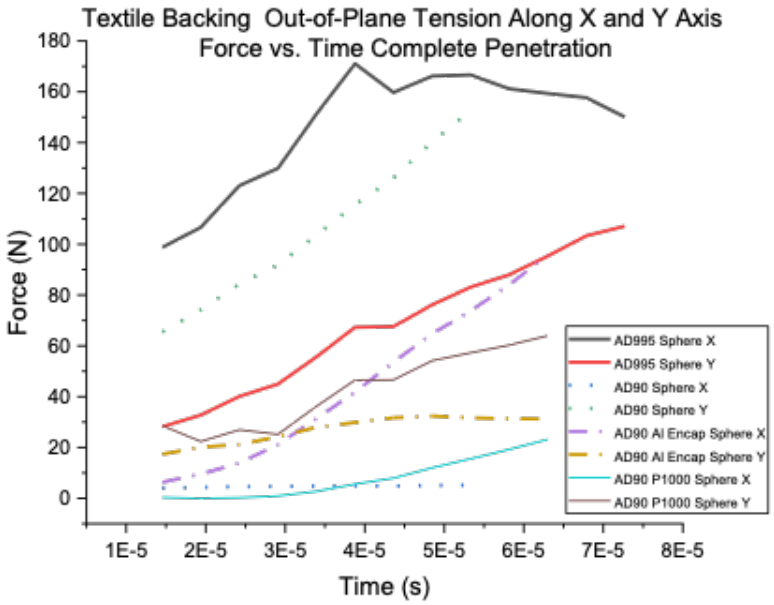

Figure 67. Tensile Force (T_p) vs. Indexed Time: 100% Penetration Projectiles.

C. THETA ANALYSIS

The non-linear progression of U and V implies that the theta value important in Smith's calculations would also be non-constant. This was examined geometrically by taking the inverse tangent of the height of the tent in the Z axis over the outward propagation in the X axis. The results are plotted by projectile type in Figures 68 and 69. Within each of the three shots, where partial penetration occurred, a reduction in the out-of-plane deflection angle is observed. This can be explained as the textile backing system begins to arrest the projectile, the kinetic energy component is reduced, and less energy is available to cause outward deflection. Within the in-plane deflection, there is no restriction on the propagation until the wave reaches the four rollers and further deflection is halted. For the majority of most impacts, the in-plane propagation wave did not reach the rollers.

An interesting comparison between shots 6 and 7, where the back face deflection between the SiC tile and the AD90 spheres were compared. The AD90 spheres displayed a larger back face deflection by about 10 degrees. The increase in back face deflection is

most likely due to the independence of one sphere with the neighboring spheres whereas the tile will distribute the energy to the surrounding area of the tile. Although the deflection was higher, it should be noted that the number of layers penetrated was only 61% of the number of layers penetrated within the SiC target system. The additional expansion of the textile backing system will reduce the force of the projectile on the textile material.

Within the complete penetrations that occurred, all four of the complete penetrations converged to a constant angle. The converging angle varied between 10 to 35 degrees and no correlation could be made to front face conditions.

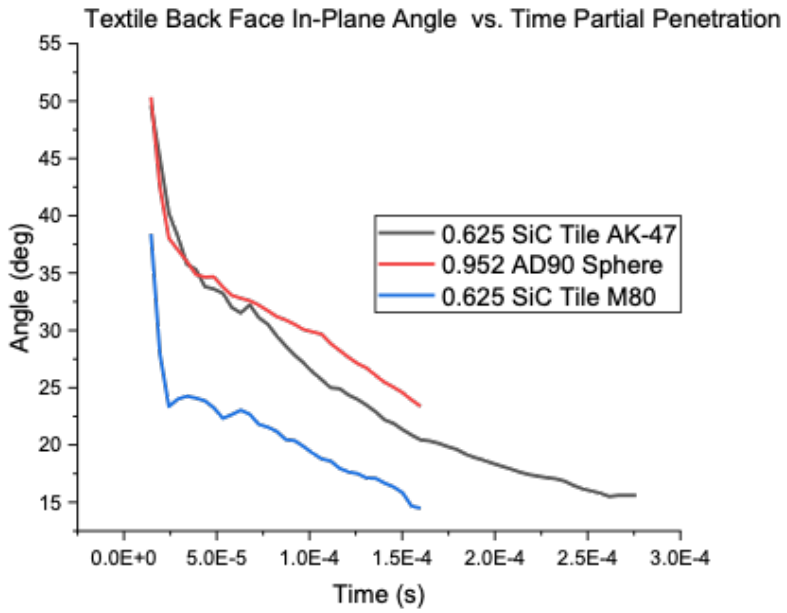

Figure 68. Deflection Angle Comparison: Stopped Projectiles.

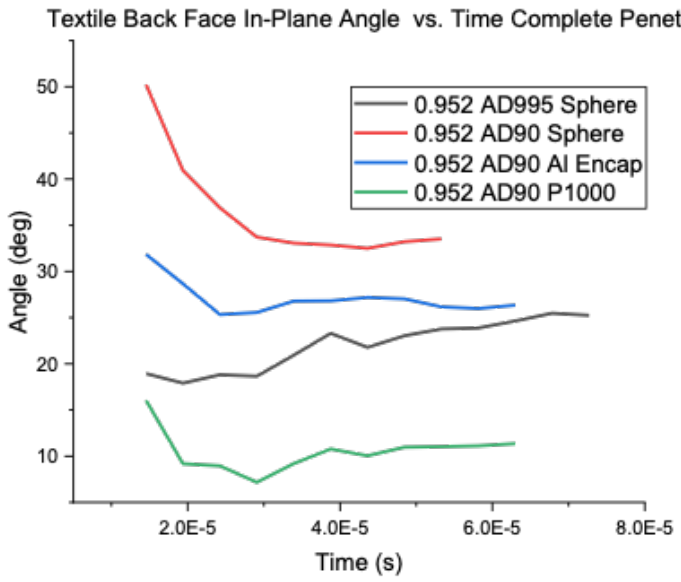

Figure 69. Deflection Angle Comparison: 100% Penetration Projectiles.

D. WORK ANALYSIS

Work analysis was performed to further understand each of the seven ballistic tests performance to dissipate the incident kinetic energy from the selected projectiles. Through investigation of the work performed by the target system on the projectile, a better understanding of how the performance of the target system performs to defeat the selected threat.

The work performed was calculated using the load cell tension along both axes (X and Y) and the out-of-plane angle of the textile to determine the out-of-plane tension. Once the force applied to the projectile is determined, the out-of-plane tension for each time step is multiplied by the distance change of the back face deflection. The sum of each time step is the total work performed on the incident projectile.

From Table 14, a large difference in work performed to dissipate incident projectile kinetic energy can be observed between partial and complete penetrations within the 7 tests performed. For the SiC tile defeating an incident AK-47 round a total of 770.6 J of energy was applied by the target system to arrest the incident projectile. For the M80 round both

the SiC tile and AD90 sphere performed just over 400 J to arrest the incident projectile. For each of the complete penetrations the work performed never exceeded 25 J and the average work was 11 J.

Based on Table 14 and Figure 62, it appears that there is a threshold pressure of the incident projectile where below this value the textile backing material will arrest the projectile and a continual reduction in the back face velocity occurs. However, if the incident pressure of the projectile exceeds a specific limit, the back face velocity increases. The increase in back face velocity is believed to be correlated to the penetration of the textile layers with minimal coupling between the backing material.

Investigating further the four different projectiles having complete penetration. Through analysis of the work, it can be determined that the AD995 spheres performed better than the AD90 spheres including the two encapsulated systems (Al and P1000).

Comparing the kinetic energy associated with the back face velocity, for each of the partial penetrations, the associated energy related to the projectile was 60% for the SiC tile against the AK-47 and 40% for both the M80 partial penetrations. The remaining energy is related to the inertial of the textile backing system.

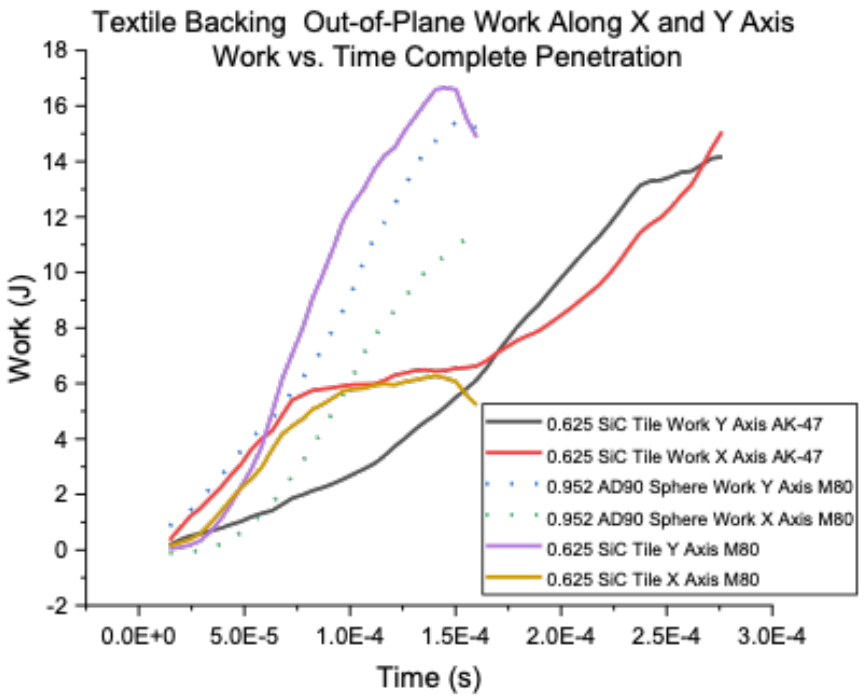

Figure 70. Work (W) Comparison: Stopped Projectiles.

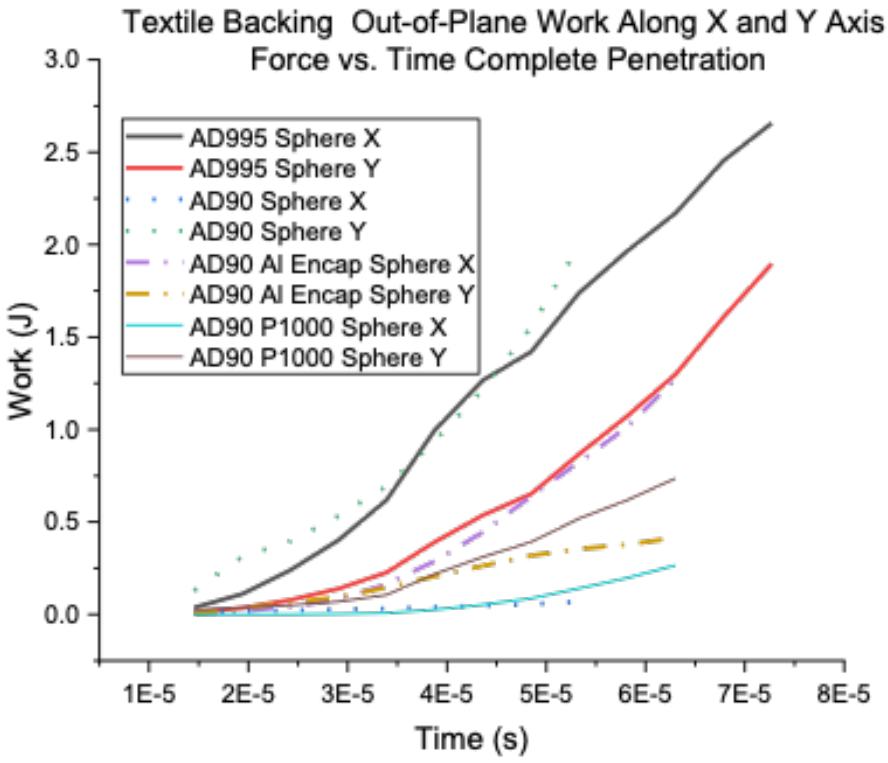

Figure 71. Work (W) Comparison: 100% Penetration Projectiles.

Table 13. Stopped Projectile Kinetic Energy Loss

Target	Back Face initial Velocity (m/s)	Back Face Final Velocity (m/s)	Kinetic Energy Lost (J)
SiC Tile AK	343.7	0	464
AD90 Sphere M80	198.2	0	188.56
SiC Tile M80	192.8	0	178.42

Table 14. Work Performed by All Targets

Target	Work Performed (J)	Penetration
SiC Tile AK	770.6	Partial
AD995 AK	24.8	Complete
AD90 AK	8.0773	Complete
AD90 Al Encap AK	7.065	Complete
AD90 P1000 AK	3.86	Complete
AD90 M80	402.76	Partial
SiC Tile M80	404.95	Partial

THIS PAGE INTENTIONALLY LEFT BLANK

VI. CONCLUSION

The purpose of this thesis research was to examine rapid impact ballistic loading on two-piece composite armor systems consisting of varying ceramic front faces coupled with an 80-layer Dyneema HB26 UHMWPE backing. For comparison, 0.635 cm thick SiC tiles, 0.952 cm diameter AD90 and AD995 ceramic sphere lattices (including encapsulations) were tested against both the AK-47 ball 7.62x39 mm and M80 7.62x51 mm projectiles at 4000 psi breech pressure. These experiments were analyzed both for back face deflection and load cell tension values to both correlate with Smith's work and to investigate overall armor system performance dependency on front face armor systems (tile vs. ceramic spheres).

Past research suggested that ceramic spheres would provide similar kinetic energy reduction as the commonly used SiC front face armor tiles while reducing aerial density as well as improving resistance to damage caused by daily use or multiple impacts. Given the application of the UHMWPE remains constant in each test, the final goal was testing composite body armor front face systems to determine performance variations primarily related to differences between ceramic spheres and tiles.

Analysis of the back face deflection for the textile backing was performed in both in-plane and out-of-plane directions during impact enabling determination of deformation propagation velocities both in-plane (U) and out-of-plane (V). A total of seven shots were performed incorporating two incident projectiles (AK-47 and M80) and five different front ceramic armor systems.

Within the seven shots studied, three of the impacts were partial penetrations (1, 6,7) and four were complete penetrations. Back face deflection and load cell measurements of the tensile forces were performed to gain a better understanding of the response of the back face textile armor as a function of the front face ceramic system.

The U values ranged from approximately 360 to 1200 m/s with no clear observable trends; however, for values of V it was determined that it had a range of values from 193-359 m/s and the four shots that had complete penetration had values over 250 m/s.

Load cell analysis was conducted for all shots. The load cell data for partial penetration events within shots 1, 6 and 7 reached maximum pressures of 1562 N, 1805 N, and 2360 N. Whereas for complete penetrations the highest tensile strength was 1300 N and the lowest was 750 N suggesting a much lower coupling of the projectile to the textile armor backing system.

For the M80 engagements, the AD90 ceramic sphere lattice outperformed the SiC tile in by displaying both lower force and lower laminate layers of the UHMWPE backing penetrated. This result would quantify the AD90 ceramic spheres as a desired replacement for SiC tile in terms of meeting NIJ Level III efforts while reducing aerial density, weight, and probability of crack propagation.

Deflection angle calculations over time were conducted. A key observation from deflection angle measurements was that all complete penetration deflection angles converged to a constant value, whereas all partial penetrations continued to decrease. The angle decreases in partial penetration as the back face deflection decreases as the projectile is arrested but the in-plane component is not restricted.

Measurements of the total work performed by the armor system enabled specific quantification of the performance for each armor system. Within each partial penetration the highest work values were observed. The SiC tile applied to defeat the AK-47 ball presented a performed work of 770.6 J and both M80 partial penetrations performed work just over 400J. For complete penetrations the highest work performed was only 28 J and an average work performed within the four complete penetrations of 11 J. From this study it suggests that if the incident projectile exceeds a specific pressure that minimal work is performed on the projectile.

LIST OF REFERENCES

[1] J. M. Robinson, "Performance of encapsulated ceramic spheres compared to monolithic ceramic plate," M.S. thesis, Dept. of Applied Physics, NPS, Monterey, CA, USA, 2019.

[2] E. M. Messiry, *Protective Armor Engineering Design*. Oakville, Ontario: Apple Academic Press, 2020.

[3] Committee on Review of Test Protocols Used by the DoD to Test Combat Helmets, "Review of Department of Defense Test Protocols for combat helmets," *National Center for Biotechnology Information*, 31-Mar-2014. [Online]. Available: https://www.ncbi.nlm.nih.gov/books/NBK224911/?report=classic. (accessed: Oct 21, 2021).

[4] Global Security, "Interceptor Body Armor," *Global Security Organization*. https://www.globalsecurity.org/military/systems/ground/interceptor.htm (accessed Oct. 21, 2021).

[5] National Institute of Justice, "Ballistic Resistance of Body Armor," U.S. Department of Justice, NIJ Standard 0101.06, Jul. 2008.

[6] Inspector General, DoD, "DoD Testing Requirements for Body Armor," United States Department of Defense, Washington, D.C., D-2009-047, Jan. 2009.

[7] Photograph of Round Comparison 7.62x51 vs 7.62x39, *The Ammo Club*, (accessed: Oct. 22, 2021). [Online]. Available: https://www.ammoforsale.com/ammo-club/762x51-vs-762x39-whats-the-difference/.

[8] J. Siewert, "Rifling Profile Push Tests: an Assessment of Bullet Engraving Forces in Various Rifling Designs," *Armament Research, Development and Engineering Center.* Picatinny, NJ. (accessed: Oct. 22, 2021). [Online]. Available: https://apps.dtic.mil/sti/pdfs/ADA431357.pdf.

[9] G. L. Rottman, *The AK-47: Kalashnikov-series assault rifles*. Bloomsbury Publishing, 2011.

[10] *7.62 x 39 –FMJ (V340842)–124 GRS,* Sellier & Bellot. (accessed: Oct 23, 2021). [Online]. Available: https://www.sellier-bellot.cz/en/products/rifle-ammunition/rifle-ammunition-training-fmj/detail/216/.

[11] Photograph of 7.62x39mm, 122 grain FMJ-BT, *International Ammunition Association, Inc.*, (accessed: Oct. 22, 2021). [Online]. Available: https://forum.cartridgecollectors.org/t/discussion-about-5-56x45-and-5-45x39-bullets-internal-components/36705.

[12] R. Gamache, Interviewee, *Private Communication.* [Interview]. October 2021.

[13] I. G. Crouch, G. V. Franks, C. Tallon, S. Thomas and M. Naebe, "Glasses and Ceramics," in *The Science of Armour Materials*, Elseiver Ltd, 2017.

[14] Bayville Chemical Supply Company Inc, "Versalink P-1000," Deer Park, New York.

[15] M. Walker, "Stress-strain relationships in ultra-high molecular weigth polyethylene fibers under ballistic loading," M.S. thesis, Dept. of Applied Physics, NPS, Monterey, CA, USA, 2018.

[16] J. C. Smith, F. L. McCrackin, and H. F. Schiefer, "Stress-strain relationships in yarns subjected to rapid impact loading: 5. Wave propagation in long textile yarns impacted transversely," J. Research NBS 60, 5 (1958) RP2866.

[17] B. Cheesman and T. Bogetti, "Ballistic impact into fabric and compliant composite laminates," Composite Structures, vol. 61, pp. 161–73, 2003.

[18] Photograph of Pure UHMWPE Ballistic Plate, *Shandong Protective Products Co. Ltd*, (accessed: Oct. 22, 2021). [Online]. Available: https://www.globalsources.com/si/AS/Shandong-Guard/6008848896158/pdtl/Pure-UHMWPE-Ballistic-Plate/1113682072.htm.

[19] DSM, "Dyneema HB26 specification sheet." [Online]. Available: https://www.dsm.com/

[20] OMEGA, "LCHD Load Cell Specification Sheet." [Online]. Available: https:// www.omega.com/pressure/pdf/LCHD.pdf

[21] Whithner, "Triggerbox 1000 specification sheet." [Online]. Available: www.whithner.com/images/TRIGGER-SCREEN-BROCHURE.pdf

[22] BNC, "577 Pulse Generator specification sheet." [Online]. Available: https://www.berkeleynucleonics.com/sites/default/files/products/datasheets/577-ds-5-2-18.pdf

[23] NI, "9237 Signal Conditioner specification sheet." [Online]. Available: http://www.ni.com/pdf/manuals/374186a_02.pdf

[24] Phantom, “V2512 specification sheet.” [Online]. Available: https://www.phantomhighspeed.com/Portals/0/Docs/DS/DS_WEB-UHS-vXX12-Family.pdf?ver=2017-07-11-085549-743

THIS PAGE INTENTIONALLY LEFT BLANK

INITIAL DISTRIBUTION LIST

1. Defense Technical Information Center
   Ft. Belvoir, Virginia

2. Dudley Knox Library
   Naval Postgraduate School
   Monterey, California